People`s Democratic Republic of Algeria

Ministry of Higher Education and Scientific Research

University of Echahid Hamma Lakhdar - El Oued

Faculty of Technology

Department of Mechanical Engineering

Dissertation

ACADEMIC MASTER

Domain: **Science and Technology**

Division: **Mechanical Engineering**

Specialty: **Electromechanical**

Presented by:

- **Hemici Hamza**
- **Sahraouie Mohammed Yacine**

Entitled:

Design and Optimization of a Fractional-Order PI Controller for PMSM Generator Control Using Metaheuristic Algorithms

Dissertation Submitted in Partial Fulfillment of the Requirements for the Master

MEM

Degree in Electromechanical

Publicly defended in: 14/06 /2026

Board of Examiners:

Dr. BEGGAT Feteh	Chairman
Dr. BenAmor Afaf	Supervisor
Dr. Souhaib Remha	Examiner

Academic Year : 2025-2026

ACKNOWLEDGMENTS

First and foremost, praise be to Allah, who granted me the strength, patience, and perseverance necessary to accomplish this work.

I would like to express my special gratitude to my parents for their continuous support, care, and encouragement throughout my academic journey.

I would also like to extend my sincere thanks and appreciation to my supervisor,

Dr. BenAmor Afaf, for her valuable guidance, insightful advice, and constant support, which greatly contributed to the completion of this dissertation.

I would like to express my deep gratitude to all the professors who contributed to my education throughout my years of study at the University of Echahid Hamma Lakhdar – El Oued, for the quality of education and valuable knowledge they provided.

My sincere thanks also go to the members of the examination committee for honoring me by accepting to evaluate and discuss this work.

Finally, I would like to express my heartfelt gratitude to everyone who contributed, directly or indirectly, to the completion of this dissertation.

DEDICATION

To the source of my strength and the reason for my perseverance, my beloved Parents, whose prayers and sacrifices paved the way for my success.

To my Sisters and Brothers, for their constant encouragement and for being the light during my darkest hours of study.

To all my Teachers and Mentors, who shared their knowledge and wisdom to shape my intellectual path.

To my Friends and Colleagues, with whom I shared the challenges and triumphs of this academic journey.

Finally, to everyone who believed in me when I doubted myself, and to my homeland, I dedicate this work as a symbol of gratitude and a step toward a brighter future.

Abstract

Abstract

Permanent Magnet Synchronous Motors (PMSMs) are widely used in modern drive systems due to their high efficiency, high power density, and excellent dynamic performance. This dissertation investigates the modeling and control of a PMSM supplied by a two-level voltage source inverter (2L-VSI). A review of current control techniques is presented, including PI-based control, hysteresis control, predictive current control, deadbeat predictive control, and modulated predictive control.

A mathematical model of the PMSM is developed using the abc, αβ, and dq reference-frame transformations, providing the basis for advanced control implementation. The study focuses on an advanced predictive current control strategy based on real-time current measurements and the Grey Wolf Optimizer (GWO) algorithm. Unlike conventional predictive current control, the proposed method reduces sensitivity to motor parameter variations and improves robustness.

Simulation results obtained in MATLAB/Simulink demonstrate that the proposed controller achieves fast dynamic response, accurate current tracking, reduced current ripple, and enhanced robustness under speed, load, and parameter variations. These results confirm the effectiveness of the proposed approach as a promising solution for high-performance PMSM drive applications.

Keywords:

PMSM, Predictive Current Control, Grey Wolf Optimizer, FOC, Two-Level Inverter, Robust Control.

صخلملا

تُعد المحركات المتزامنة ذات المغناطيس الدائم (MSAP/PMSM) من أكثر الآلات الكهربائية استخدامًا في أنظمة القيادة الحديثة بفضل كفاءتها العالية، وكثافة القدرة المرتفعة، وأدائها الديناميكي الممتاز. يتناول هذا العمل دراسة نمذجة والتحكم في محرك متزامن ذي مغناطيس دائم مُغذّى بواسطة عاكس ثلاثي الطور ثنائي المستويات.تم استعراض أهم تقنيات التحكم في التيار، بما في ذلك التحكم المعتمد على المنظمPI ، والتحكم بالهسترة، والتحكم التنبئي للتيار، والتحكم التنبئي من نوعDeadbeat ، والتحكم التنبئي المُعدَّل. كما تم تطوير نموذج رياضي للمحرك باستخدام تحويلات المراجع abc و αβ وdq ، مما يوفر أساسًا لتطبيق استراتيجيات التحكم المتقدمة.يركز هذا البحث على تطوير استراتيجية تحكم تنبئي متقدمة للتيار تعتمد على قياسات التيار الآنية وخوارزمية **Grey Wolf Optimizer (GWO).** وتمتاز الطريقة المقترحة بانخفاض حساسيتها لتغيرات معاملات المحرك مقارنةً بالتحكم التنبئي التقليدي، مما يعزز متانة النظام وأدائه.أظهرت نتائج المحاكاة باستخدام برنامج MATLAB/Simulink أن الاستراتيجية المقترحة تحقق استجابة ديناميكية سريعة، وتتبعًا دقيقًا للتيار، وتقليلًا لتموجات التيار، ومتانة عالية في مواجهة تغيرات السرعة وعزم الحمل ومعاملات المحرك. وتؤكد هذه النتائج فعالية الطريقة المقترحة كحل واعد لتطبيقات القيادة عالية الأداء للمحركات المتزامنة ذات المغناطيس الدائم.

ةيحاتفملا تاملكلا:

طاقة الرياح, المولد المتزامن دو المغناطيس الدائم (PMSG), التحكم الموجه بالمجال (FOC), المتحكم PI, خوارزمية الذئاب الرمادية (GWO), المنطق الضبابي, أنظمة طاقة الرياح

Résumé

Les moteurs synchrones à aimants permanents (MSAP) sont largement utilisés dans les systèmes d'entraînement modernes grâce à leur rendement élevé, leur forte densité de puissance et leurs excellentes performances dynamiques. Ce mémoire présente une étude de la modélisation et de la commande d'un MSAP alimenté par un onduleur triphasé à deux niveaux.

Une revue des principales techniques de commande du courant est d'abord réalisée, notamment la commande basée sur le régulateur PI, la commande par hystérésis, la commande prédictive du courant, la commande prédictive de type Deadbeat et la commande prédictive modulée. Par ailleurs, un modèle mathématique du MSAP est développé à l'aide des transformations de repère abc, αβ et dq, constituant ainsi une base solide pour la mise en œuvre des stratégies de commande avancées.

Ce travail s'intéresse particulièrement à une stratégie avancée de commande prédictive du courant basée sur les mesures de courant en temps réel et l'algorithme d'optimisation Grey Wolf Optimizer (GWO). Contrairement à la commande prédictive classique, l'approche proposée présente une faible sensibilité aux variations des paramètres de la machine, ce qui améliore la robustesse et les performances globales du système.

Les résultats de simulation obtenus sous MATLAB/Simulink montrent que la méthode proposée assure une réponse dynamique rapide, un suivi précis des courants, une réduction des ondulations de courant ainsi qu'une grande robustesse face aux variations de vitesse, de couple de charge et des paramètres du moteur. Ces résultats confirment l'efficacité de la stratégie proposée et son potentiel pour les applications d'entraînement à hautes performances basées sur les MSAP.

Mots-clés : MSAP, commande prédictive du courant, Grey Wolf Optimizer (GWO), commande orientée champ (FOC), onduleur triphasé à deux niveaux, commande robuste.

Contents

Contents

Contents

List of figures

List of figures

List of Symbols

Symbol	Description	Unit
(V_a, V_b, V_c)	Stator phase voltages	V
(I_a, I_b, I_c)	Stator phase currents	A
(V_d, V_q)	Direct and quadrature axis voltages	V
(I_d, I_q)	Direct and quadrature axis currents	A
(R_s)	Stator resistance	Ω
(L_d)	Direct-axis inductance	H
(L_q)	Quadrature-axis inductance	H
(φ_d)	Flux linkage along d-axis	Wb
(φ_q)	Flux linkage along q-axis	Wb
(φ_f)	Permanent magnet flux linkage	Wb
(T_e)	Electromagnetic torque	N·m
(T_m)	Mechanical torque	N·m
(T_L)	Load torque	N·m
(J)	Moment of inertia	$kg \cdot m^2$
(f)	Viscous friction coefficient	N·m·s/rad
(ω_m)	Mechanical angular speed	rad/s
(ω_e)	Electrical angular speed	rad/s
(P)	Number of pole pairs	–
(θ_e)	Electrical rotor angle	rad
(P_e)	Electrical power	W
(P_m)	Mechanical power	W
(P_{em})	Electromagnetic power	W
(λ)	Tip-speed ratio	–
(β)	Blade pitch angle	°
(C_p)	Power coefficient	–
(P_{wind})	Available wind power	W
(P_{aero})	Aerodynamic power	W
(T_{aero})	Aerodynamic torque	N·m
(V_w)	Wind speed	m/s
(R)	Turbine blade radius	m
(S)	Swept area of turbine	m^2
(ρ)	Air density	kg/m^3
(k)	Gearbox ratio	–
(f_e)	Electrical frequency	Hz
(n)	Rotor speed	rpm
(V_{dc})	DC bus voltage	V

Abbreviations

Abbreviation	Meaning
PMSM	Permanent Magnet Synchronous Machine
PMSG	Permanent Magnet Synchronous Generator
FOC	Field Oriented Control
PI	Proportional Integral
GWO	Grey Wolf Optimization
FL	Fuzzy Logic
PWM	Pulse Width Modulation
AC	Alternating Current
DC	Direct Current
MPPT	Maximum Power Point Tracking
dq	Direct-Quadrature Reference Frame

General Introduction

General Introduction

In recent decades, electric drive systems have experienced remarkable development thanks to advances in power electronics, microprocessors, and advanced control techniques. These improvements have enabled the design of more efficient, high-performance systems that meet the increasing demands of modern industrial applications. In this context, Permanent Magnet Synchronous Motors (PMSMs) have emerged as a preferred solution in various fields such as electric vehicles, renewable energy systems, robotics, and high-performance industrial drives. Their success is mainly due to their high efficiency, high power density, excellent dynamic behavior, and low maintenance requirements.

However, achieving optimal performance from these machines requires the implementation of advanced control strategies capable of ensuring fast dynamic response, accurate tracking, and strong robustness against external disturbances and parameter uncertainties. Among the most widely used approaches, Field-Oriented Control (FOC) is considered a benchmark technique due to its ability to decouple flux and torque control, providing performance comparable to DC machines. Nevertheless, this method has certain limitations, particularly its sensitivity to parameter variations and the complexity of its control structure.

To overcome these limitations, recent research has focused on advanced control techniques, especially predictive control methods. These approaches rely on a system model to predict future behavior and determine the optimal control action at each sampling period. Among the different variants reported in the literature are Model Predictive Current Control (MPCC), Deadbeat predictive control, and modulated predictive control strategies. These methods are characterized by fast dynamic response, conceptual simplicity, and the ability to directly incorporate system constraints into the control process.

However, the performance of classical predictive control remains highly dependent on the accuracy of the motor parameters used in the prediction model. Any variation in electrical parameters, particularly stator resistance and inductances, can significantly degrade control performance. To address this issue, recent approaches have introduced intelligent optimization-based techniques. Among them, the Grey Wolf Optimizer (GWO) algorithm has shown strong potential due to its ability to efficiently search for optimal solutions while maintaining relatively low computational complexity.

In this context, accurate system modeling is a fundamental step for the design, analysis, and evaluation of control strategies. This modeling includes both the Permanent Magnet

Synchronous Motor and the two-level three-phase voltage source inverter that supplies the machine. Reference frame transformations (abc, αβ, and dq) are used to simplify system equations and facilitate the implementation of advanced control laws. In addition, both continuous-time and discrete-time models are essential for the digital implementation of predictive control algorithms.

The main objective of this thesis is to study, model, and compare different current control strategies applied to PMSMs, with particular emphasis on predictive control techniques. An advanced predictive current control strategy based on real-time current measurements and the Grey Wolf Optimizer algorithm is proposed to improve system robustness against parameter variations while maintaining excellent dynamic performance.

This thesis is organized as follows:

- **Chapter 1** presents a state-of-the-art review of different current control methods applied to PMSMs, highlighting their principles, advantages, and limitations.
- **Chapter 2** is devoted to the detailed modeling of the drive system consisting of a PMSM supplied by a two-level voltage source inverter. Reference frame transformations, dynamic models, and energy equations are developed.
- **Chapter 3** introduces the proposed advanced predictive current control strategy based on the Grey Wolf Optimizer (GWO). Its operating principle is described, and its performance is evaluated through simulation and compared with classical predictive control methods.

Chapter I

Wind Energy Conversion System Based on a Permanent Magnet Synchronous Machine (PMSM)

I.1 Introduction:

Synchronous machines are key electrical components in modern industrial systems, mainly due to their high efficiency and their ability to operate at a constant speed strictly synchronized with the supply frequency. The differences between these machines are essentially based on the excitation method used. Among them, the permanent magnet synchronous motor (PMSM) stands out for its excellent performance, high power density, and compact design. These features make synchronous machines essential elements in a wide range of advanced industrial and technological applications, particularly in wind energy systems.

This chapter presents a detailed study of synchronous machines, with a particular focus on the permanent magnet synchronous motor (PMSM). It first covers the historical development, fundamental operating principles, internal structure, and main application areas of PMSMs. It then explores various control strategies, including both classical approaches and modern optimization-based control techniques.

Ⅰ.2 Wind Energy System

I.2.1 General about Wind Energy

Wind energy corresponds to the kinetic energy of moving air, whose driving force can be exploited to propel sailboats and other types of vehicles. Alternatively, this kinetic energy can be converted into useful energy forms using an aerogenerator such as a wind turbine or a traditional windmill. It is widely recognized as an important renewable energy source.

The use of wind energy can be classified into three main applications. First, it can be directly used as mechanical energy, where wind is employed to propel vehicles such as sailing boats or land vehicles like wind-powered cars. This mechanical energy has also historically been used for water management tasks, as seen in traditional mills, for operating wind-driven pumps used in irrigation and livestock watering, and for grinding grain using millstones.

Second, wind energy can be converted into mechanical motive power for processes such as pumping fluids or compressing gases.

Third, it is widely applied in electricity generation, where a wind turbine is mechanically coupled to an electrical generator to produce either direct current (DC) or alternating current (AC). The generated electricity can be supplied to the electrical grid or used in standalone systems, which often include backup sources such as diesel generators as well as energy storage systems, typically battery banks or other storage technologies [1]

I.2.2 Wind Energy System components

A wind turbine consists of multiple complex subsystems that work together to convert the kinetic energy of the wind into electrical energy. Each component is designed to perform a specific function, and their coordinated operation ensures the overall efficiency and reliability of the system in producing electricity. [2]

Generally, wind turbines are composed of four principal sections:

• The Rotor Blades

• The Nacelle

• The Generator Assembly

• The Tower

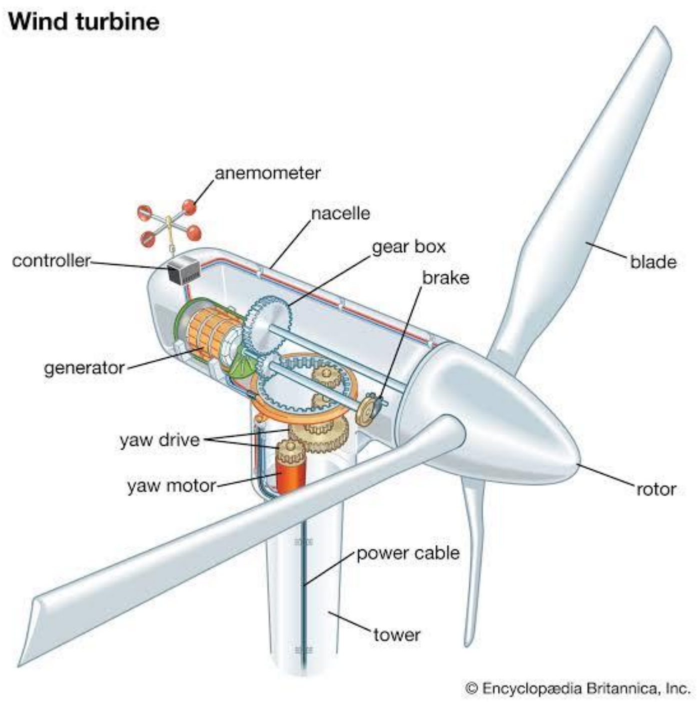

Figure I.1. Components of a Wind Turbine.

I.2.3 Operating principle

Using a device known as a wind turbine (Figure I.1), or windmill, wind energy is converted from kinetic energy into mechanical power transmitted through a drive shaft. This mechanical power is then transformed into electrical energy by coupling the shaft to an electric generator. The resulting alternating current is subsequently conditioned using static power electronic converters, typically by rectifying it into direct current and, when necessary, inverting it back into alternating current. This allows the energy to be either stored in batteries or directly injected into the electrical grid. In this configuration, the system is commonly referred to as an aerogenerator. [3]

I.2.4 State of the Art on Electromechanical Conversion

The wind turbine converts the kinetic energy of wind into mechanical power. A gearbox is often employed to adjust the low rotational speed of the turbine (typically around 10–200 rpm) to the higher operating speed required by conventional generators (generally 750–3000 rpm). The generator then transforms this mechanical input into electrical energy, which can be delivered to the electrical grid either through a direct or an indirect connection.

In the case of direct grid connection, the generator operates at a fixed or nearly fixed rotational speed, usually achieved by controlling the slip of an asynchronous machine. In contrast, indirect connection uses power electronic converters between the generator and the grid, thereby decoupling the mechanical speed of the machine from the grid frequency. This configuration enables variable-speed operation and allows the use of synchronous machines, asynchronous machines, or other specialized topologies, ultimately improving the overall energy conversion efficiency of the system. [2]

Variable-speed operation can also enhance the quality of the generated electrical power, as it offers greater flexibility in handling rapid fluctuations in wind speed. Within this context, variable-speed wind turbines equipped with permanent magnet synchronous generators (PMSGs) have attracted increasing attention in recent years from wind turbine manufacturers [3].

Since the rotor's permanent magnets provide the excitation flux, no stator magnetizing current is required to establish the air-gap flux. As a result, the stator current is mainly devoted to torque production [4]. Consequently, for a given power output, a PMSG achieves a higher power factor and generally demonstrates higher efficiency compared to induction generators used in other wind turbine configurations.

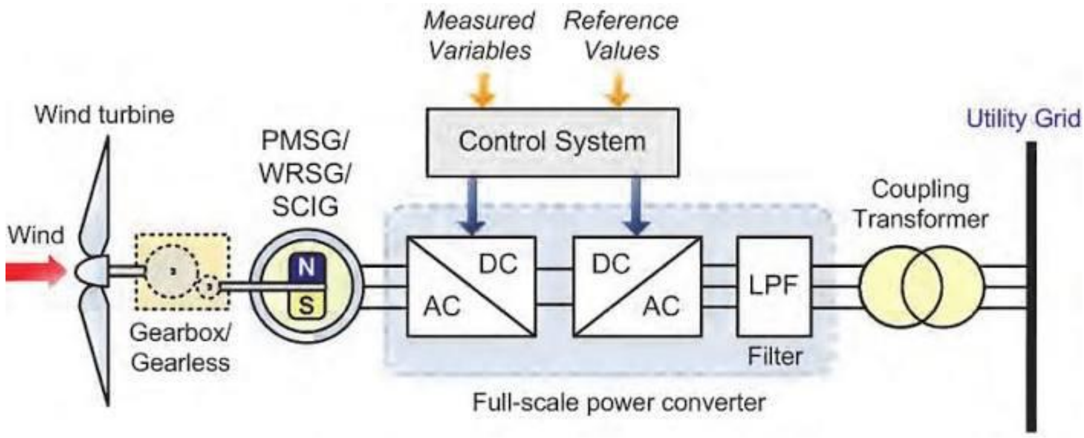

Figure I.2. Wind Turbine with a Permanent.

I.3 Permanent magnet synchronous machine

Focusing on this class of synchronous machines, permanent magnet synchronous machines (PMSMs) are high-efficiency AC motors that employ strong permanent magnets in the rotor instead of conventional excitation windings. This configuration eliminates rotor copper losses, resulting in higher torque density and a more compact machine design.

The late 1980s marked the beginning of the brushless permanent magnet motor era, largely enabled by advances in power electronics and the development of high-energy-density rare-earth magnets. Since then, PMSMs have emerged as a more efficient and reliable alternative to conventional induction motors, particularly in the context of growing demand for low-carbon and green energy technologies. [5]

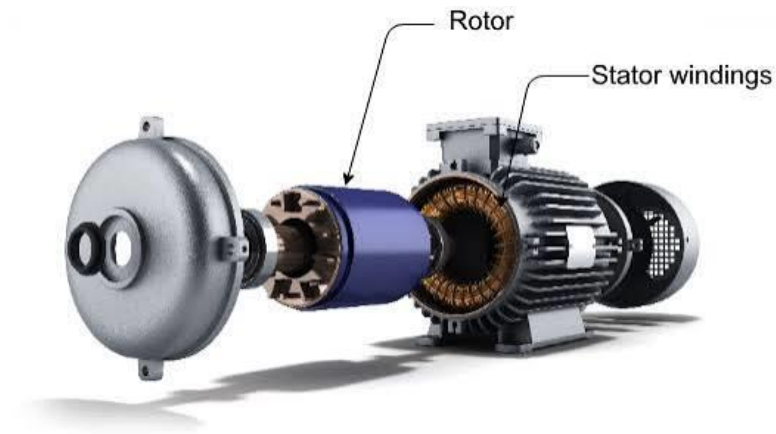

Figure I.3. Permanent magnet synchrones machine.

Among the most important characteristics of permanent magnet synchronous machines (PMSM).

- High efficiency and high torque: provides power equivalent to two to four times that of induction motors of the same size.
- Precise control: allows precise control of speed and position.
- High power density: excellent torque-to-weight ratio.
- No need excitation coils: the permanent magnet self-generates the magnetic field, which reduces the Heat lost and improves the efficiency (energy saving).
- Low maintenance: due to the absence of brushes and commutators.

I.3.1 Components of (PMSM)

Like all electrical machines, permanent magnet synchronous machines are mainly composed of a stationary part (the stator) and a rotating part (the rotor), along with various auxiliary components that ensure proper operation and performance.

I.3.1.1 Stator

The stator of a permanent magnet synchronous machine resembles that of an asynchronous machine. It is composed of stacked magnetic sheets, which feature slots housing three identical windings spaced 2π/3 apart.

Figure I.4 Stator of machine PMSM

I.3.1.2 Rotor

The rotor in a Surface-Mounted Permanent Magnet Synchronous Machine (SMPMSM) typically comes in two forms:

- A rotor that has pole pieces. These focus the magnetic flux, and the magnets are arranged either parallel or perpendicular to the air gap, or in a more complex way. In this machine type, the inductor has jn
- A rotor without pole pieces, so it has a constant air gap where the magnets' magnetization is commonly perpendicular to the air gap.

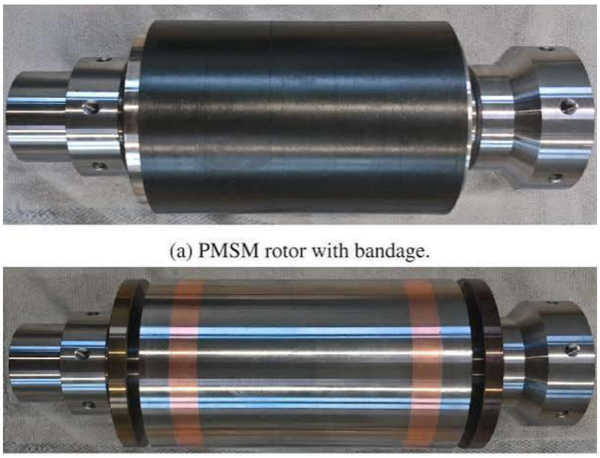

(a) PMSM rotor with bandage.

(b) IM rotor with retaining rings.

Figure I.5. Rotor of machine PMSM.

I.3.2 Operating Principle of (PMSM)

The operation of a permanent magnet synchronous motor is based on the interaction between the rotor's permanent magnetic field and the stator's electromagnetic field. When alternating current flows through the stator windings, it generates a rotating magnetic field. The rotor's permanent magnets interact with this rotating field, producing electromagnetic forces that cause the rotor to turn. The rotor rotates at exactly the same speed as the stator's magnetic field, with no slip between them, which is why the machine is referred to as synchronous [6].

A PMSM converts electrical energy into mechanical energy through the interaction of two magnetic fields: one produced by the permanent magnets mounted on the rotor, and the other generated in the stator when it is supplied with alternating current [7].

The operating principle can be described in the following steps. First, the stator windings carry AC current, which creates a rotating magnetic field whose speed depends on the supply frequency. Second, the rotor, equipped with permanent magnets, generates a constant magnetic field. Third, the interaction between these two fields produces electromagnetic torque due to attraction and repulsion between opposite and like poles, causing the rotor to rotate. Finally, the rotor follows the stator's rotating field at synchronous speed.

What characterizes this operation as synchronous is that the rotor speed is locked to the rotating magnetic field of the stator. Unlike in induction machines, there is no slip between the two speeds. In induction motors, a slight speed difference is necessary to induce current in the rotor and generate torque, whereas in PMSMs the rotor is directly coupled to the magnetic field created by the stator, eliminating slip entirely [3].

In summary, a permanent magnet synchronous motor operates by continuously aligning the rotor's permanent magnetic field with the stator's rotating magnetic field. This direct magnetic coupling enables precise speed control, high efficiency, and effective energy conversion.

field made by the stator. Because of this direct link, the motor provides accurate speed control and efficient turning of energy.

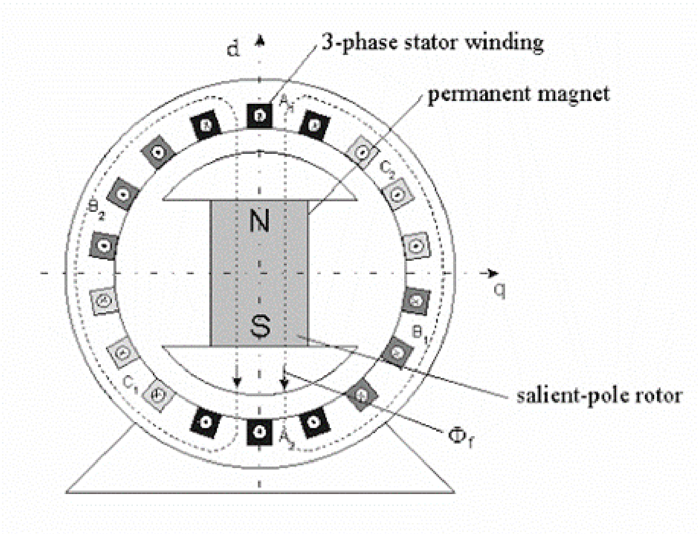

Figure I.6. Schematic Diagram of machine (PMSM).

I.3.3 Uses of the permanent magnet synchronous machine (PMSM)

Permanent magnet synchronous machines (PMSMs) are among the most widely used electrical machines in industrial and technological applications, owing to their high efficiency, high power density, fast dynamic response, and precise speed and torque control capabilities. Advances in power electronics and digital control technologies have significantly contributed to the expansion of their use across a wide range of modern engineering fields [5]. They are extensively applied in industrial automation and robotics, and are also a preferred solution in electric and hybrid vehicle propulsion systems due to their superior performance and energy efficiency. In addition, PMSMs are used as generators in renewable energy systems because of their ability to operate efficiently at low rotational speeds. They are also increasingly integrated into aerospace, marine systems, and modern household appliances equipped with inverter technology, where they help enhance performance while reducing energy consumption.

• Industrial applications and robotics: PMSMs are widely used in automation systems and precision robotic applications due to their excellent capability for accurate speed and torque control.

• Electric and hybrid vehicles: They are considered an optimal choice for electric vehicle propulsion because of their high energy density, high efficiency, and compact size, contributing to improved energy savings.

• Centrifuge systems and pumps: They are used in applications requiring high rotational speeds and stable torque, such as medical and industrial centrifuges.

• Aerospace and defense: PMSMs are employed in flight control systems and mechanical actuators due to their lightweight design, precision, and high reliability.

• Household appliances and HVAC systems: They are widely used in inverter-based compressors for air conditioners and refrigerators, providing improved energy efficiency.

• Renewable energy systems: They are used as generators in small and medium-sized wind turbines, where they offer efficient performance even at low rotational speeds.

I.4 Modeling of the permanent magnet synchronous machine

I.4.1 Description

Synchronous machines with respect to asynchronous machines have a greater power by weight. Since the rotor flow is known, it is easier to control the torque.

The progress made in the manufacture of magnets, whether based on metal alloys or rare earths, means that today the use of PMSM is increasing [6].

The permanent magnet synchronous machine (PMSM) represented by fig (I.3) comprises a stator and a rotor of symmetrical constitution with a pair of poles. In notches regularly distributed on the internal surface of the stator are housed three identical windings, their axes are spaced apart from each other by an electrical angle equal to ($2\pi/3$) and connected in a star with isolated neutral.

I.4.2 Problems of modeling

The unified theory of classical electrical machines, also called generalized theory, is based on the Park transformation which relates the stator and rotor electrical equations to the electrically perpendicular axes called d, for direct, and q for quadrature. These two axes are used, for example in Blondel's theory of synchronous machines and linked to the rotor. The d axis is the polar axis and the q axis is the interpolar axis [6].

The modeling of machines and converters in dynamic mode is also a mandatory passage, whether in continuous models with transfer functions or correcting equations or the determination of numerical control calculation algorithms.

The model of alternating current machines is much more complex than that of direct current machines and their control will be more complex, due to the fact that [8], [6] :

- All the quantities are alternating, fixed or variable frequency.
- But The degree of the electromechanical system is usually higher than that of systems based on direct current machines.
- In the systems and nonlinear with variable coefficients and multiple inputs and outputs.
- There can be four types of synchronous machine :
- A synchronous machine with a wound rotor and a smooth air gap ($Ld = Lq$).
- Synchronous machine with wound rotor and protruding pole ($Ld > Lq$), (effect of salience, increase in max torque).
- A synchronous machine with permanent magnets mounted on the surface of the rotor without pole pieces ($Ld = Lq$), (large air gap, we can have a trapezoidal torque),
- Synchronous machine parts buried in the rotor, ($Ld < Lq$), (possibility of high rotation speeds).

For our case, we are interested in the study, modeling and control of the latest variant of the synchronous machines mentioned above.

I.4.3 Simplifying assumptions

The electrical and dynamic behavior of electrical machines can only be studied if it is defined by a mathematical model. To obtain this model, the following simplifying assumptions are taken into account [7] [5] [9]:

However, the air gap is of uniform thickness, and of negligible notching.

During the saturation of the magnetic circuit, the hysteresis and the eddy currents are negligible.

However, the resistances of the windings do not vary with the temperature and the skin effect is negligible.

Thus, it is assumed that the FMM created by each of the phases of the two armatures is sinusoidally distributed.

I.4.4 Characteristic of the PMSM

A synchronous machine with a rare earth permanent magnet, which generates a constant excitation flow to the rotor (φ_f).

The machine is not equipped with a shock absorber.

All the magnets are buried in the rotor with an inverted salience, therefore the natural inductances of the stator along the axes d and q are different ($L_d > L_q$) [6].

I.5 Putting the synchronous machine into an equation

To establish simple relationships between the motor supply voltages and these currents, we consider the following ideal synchronous machine model.

I .5.1 Choice of the Repository

The Park reference frame (d,q) linked to the rotor [8], [10] is chosen.

Where ω is the pulsation of the stator quantities in the system (d,q).

I.5.2 Model of the PMSM in the Park repository

The Park transformation brings the stator equations back into a frame of reference linked to the rotor. So the equivalent machine is identical to a direct current machine having the winding f as an inductor and having two quadrature armatures. [11.30]

I.5.3 Equations of the PMSM

I.5.3.1 Stator Voltage Equations

For a three-phase PMSM, the stator voltage equations in phase variables are derived from Kirchhoff's voltage law.

For each phase:

$$v_a = R_s i_a + \frac{d\varphi_a}{dt} \qquad \text{(I.1)}$$

$$v_b = R_s i_b + \frac{d\varphi_b}{dt} \qquad \text{(I.2)}$$

$$v_c = R_s i_c + \frac{d\varphi_c}{dt} \qquad \text{(I.3)}$$

Where:

- v_a, v_b, v_c are stator phase voltages
- i_a, i_b, i_c are stator phase currents
- R_s is stator resistance
- $\varphi_a, \varphi_b, \varphi_c$ are stator flux linkages

In matrix form:

$$v_{abc} = R_s i_{abc} + \frac{d}{dt}\varphi_{abc} \tag{I.4}$$

I.5.4 Flux Linkage Expressions

The stator flux linkage consists of two components:

1. Self and mutual inductance flux
2. Rotor permanent magnet flux

Thus:

$$\varphi_{abc} = L_{abc} i_{abc} + \varphi_{pm} \tag{I.5}$$

Where:

- $\mathbf{L}_{abc}$ is the inductance matrix
- $\boldsymbol{\varphi}_{pm}$ is rotor permanent magnet flux vector

For a symmetric three-phase machine:

$$\mathbf{L}_{abc} = \begin{bmatrix} L_s & M & M \\ M & L_s & M \\ M & M & L_s \end{bmatrix} \tag{I.6}$$

Where:

- L_s= self inductance
- M= mutual inductance

I.5.5 Permanent Magnet Flux in abc Frame

The rotor magnet flux depends on rotor electrical position θ_e.

$$\varphi_{pm,a} = \varphi_f \cos(\theta_e) \tag{I.7}$$

$$\varphi_{pm,b} = \varphi_f \cos\left(\theta_e - \frac{2\pi}{3}\right) \tag{I.8}$$

$$\varphi_{pm,c} = \varphi_f \cos\left(\theta_e + \frac{2\pi}{3}\right) \tag{I.9}$$

Where:

- φ_f= permanent magnet flux linkage
- $\theta_e = p\theta_m$(electrical angle)

- p= number of pole pairs

I.5.6 Complete Voltage Equation

Substituting flux into voltage equation:

$$\mathrm{v}_{abc} = R_s \mathrm{i}_{abc} + \mathrm{L}_{abc}\frac{d\mathrm{i}_{abc}}{dt} + \frac{d\varphi_{pm}}{dt} \tag{I.10}$$

This represents the complete stator electrical model in the natural frame.

I.6 Clarke Transformation (abc → αβ)

To simplify the model, we apply Clarke transformation.

$$\begin{bmatrix} i_\alpha \\ i_\beta \end{bmatrix} = \frac{2}{3}\begin{bmatrix} 1 & -\frac{1}{2} & -\frac{1}{2} \\ 0 & \frac{\sqrt{3}}{2} & -\frac{\sqrt{3}}{2} \end{bmatrix}\begin{bmatrix} i_a \\ i_b \\ i_c \end{bmatrix} \tag{I.11}$$

Similarly for voltages and fluxes.

This converts the three-phase system into two orthogonal stationary components.

I.7 Park Transformation (αβ → dq)

The rotating reference frame is defined by angle θ_e.

$$\begin{bmatrix} i_d \\ i_q \end{bmatrix} = \begin{bmatrix} \cos\theta_e & \sin\theta_e \\ -\sin\theta_e & \cos\theta_e \end{bmatrix}\begin{bmatrix} i_\alpha \\ i_\beta \end{bmatrix} \tag{I.12}$$

This transformation eliminates time-varying inductances.

I.8 PMSM Model in dq Reference Frame

After transformation, voltage equations become:

$$v_d = R_s i_d + L_d\frac{di_d}{dt} - \omega_e L_q i_q \tag{I.13}$$

$$v_q = R_s i_q + L_q\frac{di_q}{dt} + \omega_e L_d i_d + \omega_e \lambda_f \tag{I.14}$$

Where:

- L_d, L_q= dq inductances
- $\omega_e = p\omega_m$

I.9 Electromagnetic Torque Derivation

The electromagnetic torque is derived from co-energy:

Substituting flux:

$$\varphi_d = L_d i_d + \varphi_f \quad (I.15)$$

$$\varphi_q = L_q i_q \quad (I.16)$$

Thus:

$$T_e = \frac{3}{2} p\left[\varphi_f i_q + (L_d - L_q) i_d i_q\right] \quad (I.17)$$

For Surface PMSM:

$$L_d = L_q$$

Then torque simplifies to:

$$T_e = \frac{3}{2} p \varphi_f i_q$$

I.10 Mechanical Model

Using Newton's second law for rotation:

$$J \frac{d\omega_m}{dt} = T_e - T_L - B\omega_m \quad (I.19)$$

Where:

- J= moment of inertia
- B= friction coefficient
- T_L= load torque

Electrical and mechanical speeds are related by:

$$\omega_e = p\omega_m \quad (I.20)$$

I.11 Complete State-Space Model

The state variables are:

$$x = [i_d, i_q, \omega_m]^T \quad (I.21)$$

Electrical equations:

$$\frac{di_d}{dt} = \frac{1}{L_d}(v_d - R_s i_d + \omega_e L_q i_q) \quad (I.22)$$

$$\frac{di_q}{dt} = \frac{1}{L_q}(v_q - R_s i_q - \omega_e L_d i_d - \omega_e \lambda_f) \quad (I.23)$$

Mechanical equation:

$$\frac{d\omega_m}{dt} = \frac{1}{J}(T_e - T_L - B\omega_m) \quad (I.24)$$

These last equations constitute the basis of the block diagram of the PMSM.

The frequency of the stator currents is controlled according to the rotor's rotational motion in order to maintain synchronism between the stator-generated magnetic field and the rotor magnetic moment. Consequently, the stator field rotates at the same speed as the rotor. When the rotor is at standstill, the stator field also becomes stationary. This operating principle is commonly referred to as self-synchronization or autopilot control.

I.12 Principes de base de la commande des MSAP

Since PMSMs are synchronous machines, precise torque can only be produced when the AC excitation frequency is accurately synchronized with the rotor frequency. Therefore, the fundamental requirement in PMSM control design is to ensure precise synchronization of the machine excitation with the rotor frequency. The direct approach to meeting this requirement is to continuously measure the absolute angular position of the rotor and adjust the machine excitation accordingly, as shown in Figure 1.7. This concept is also known as self-synchronization [3] and guarantees that the PMSM does not lose synchronism during operation.

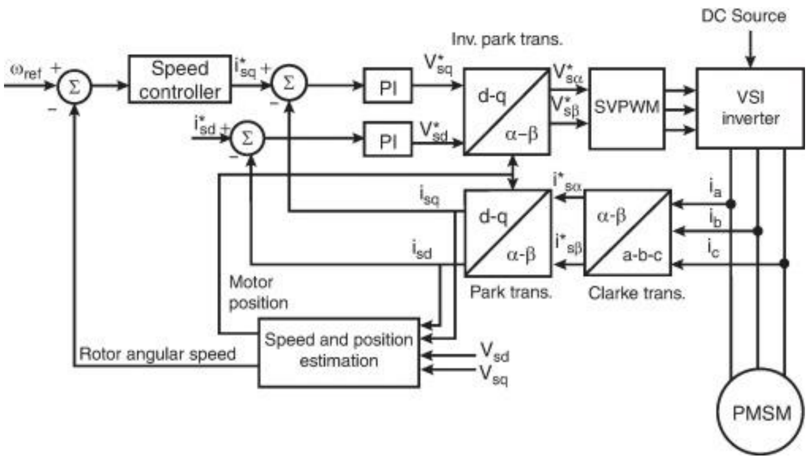

Figure I.7. Surface-Mounted Permanent Magnet Synchronous Motor (SPMSM) Structure [1].

1.12.1 Basic Control Methods of PMSMs

1.12.1.1 Scalar V/f Control

It is possible to design Interior Permanent Magnet Synchronous Motors (IPMSMs) equipped with squirrel-cage windings (damper windings) in the rotor, as shown in Figure 1.8. These squirrel-cage rotor windings are similar to those used in squirrel-cage induction motors and produce asynchronous torque whenever the IPM rotor does not rotate at synchronous speed.

The asynchronous torque generated by the squirrel-cage rotor windings during asynchronous operation brings the IPM rotor back into synchronous operation, thereby ensuring synchronous operation of the IPMSM at all times. This feature makes it possible to use a simple open-loop V/f control algorithm for this type of IPMSM, as illustrated in Figure 1.8, to achieve speed regulation in applications such as pumps and fans that do not require a fast dynamic response [1].

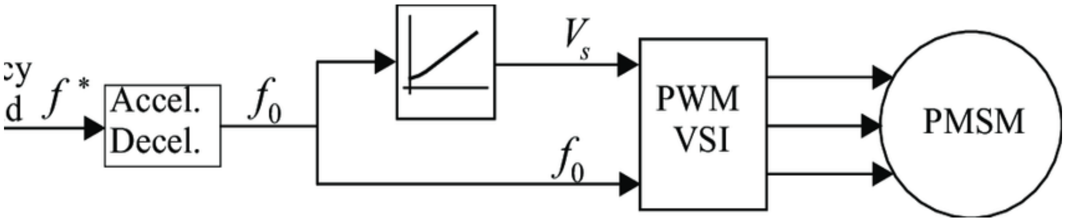

Figure I.8 illustrates the open-loop V/f control strategy, which can be applied to IPMSM motors with a squirrel-cage rotor [1].

Figure 1.4 illustrates the V/f control approach for IPMSMs with squirrel-cage rotors. This approach is similar to the V/f control (scalar control) used in induction machines. However, one of the advantages of this drive system is that the rotor speed depends only on the machine excitation frequency and does not require slip compensation, unlike induction motor drives.

While IPMSMs equipped with squirrel-cage rotor windings can be controlled using the configuration shown in Figure 1.8, difficulties may arise when controlling PMSMs without squirrel-cage rotor windings using the same control configuration. The absence of squirrel-cage rotor windings means that the machine cannot guarantee synchronization between the rotor and the excitation frequency, nor can it ensure stable operation.

Therefore, the use of the V/f control approach with PMSMs that do not have squirrel-cage rotor windings requires information about the rotor frequency (rotor speed) to maintain synchronization between the AC excitation frequency and the rotor frequency. In this case, the system must be designed to operate in a closed-loop configuration, as illustrated in Figure 1.9.

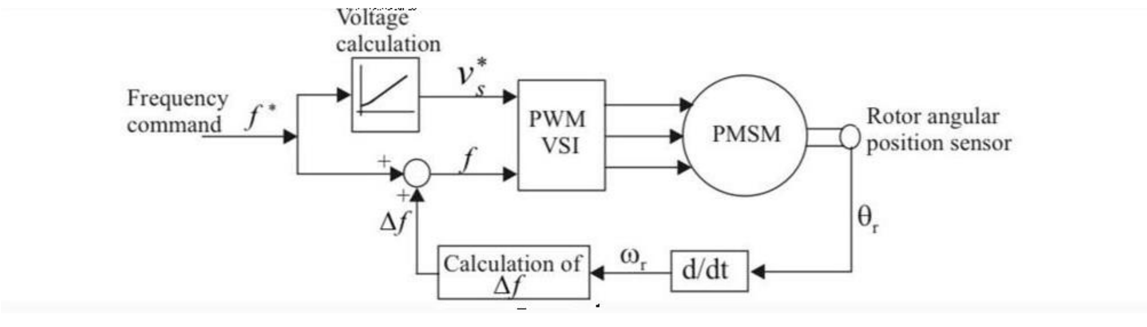

Figure I.9. V/f Control Approach for Permanent Magnet Motors without Squirrel-Cage Rotor Windings [1].

1.12.1.2 Closed-loop speed and torque control

Improved performance compared to the V/f control approach can be achieved by incorporating both torque and speed control of the machine within the drive controller. The drive control structure with torque and speed regulators is illustrated in Figure 1.6. The torque production of permanent magnet machines is directly related to the stator currents; therefore, torque control involves regulating the stator currents, which requires current feedback to be supplied to the torque controller, as shown in Fig. I.10. In addition, as discussed earlier in this section, rotor position feedback is also essential for the torque controller in order to achieve self-synchronization.

Stator current control is performed in a field-oriented reference frame within the torque controller. As a result, this type of control strategy for PMS machines is also referred to as field-oriented control (FOC).

Speed control is implemented by closing an outer speed feedback loop around the inner torque control loop, as shown in Figure 1.6. Speed feedback can be obtained using the same rotor position sensor used for rotor position estimation.

In order to achieve fast torque response, direct torque control (DTC) of PMSM drives has also attracted considerable interest in recent years. DTC requires accurate estimation of magnetic flux and torque. A detailed analysis of PMSM-based DTC is provided in [4].

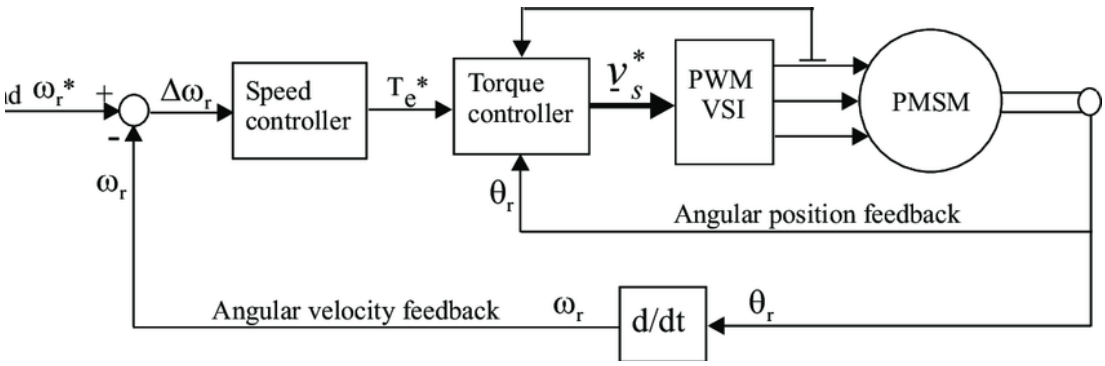

Figure I.10. Functional Diagram of a Permanent Magnet Synchronous Motor (PMSM) Control System Incorporating Torque and Speed Controllers [1].

1.13 Current Control Techniques for Permanent Magnet Synchronous Motors (PMSMs)

1.13.1 Linear Current Control Based on a PI Controller

Figure 1.11 illustrates a linear control method employing a Proportional–Integral (PI) controller and a modulation stage. The control loop generates a reference speed. The measured motor speed is compared with the reference speed, and the resulting error is fed into the PI controller.

The PI controller generates the motor reference currents. The measured motor currents are then compared with the reference currents, and the resulting current error is applied to the input of the PI controller. The PI controller processes the current error and generates a reference voltage (also referred to as the modulation waveform), which is supplied to the modulation stage.

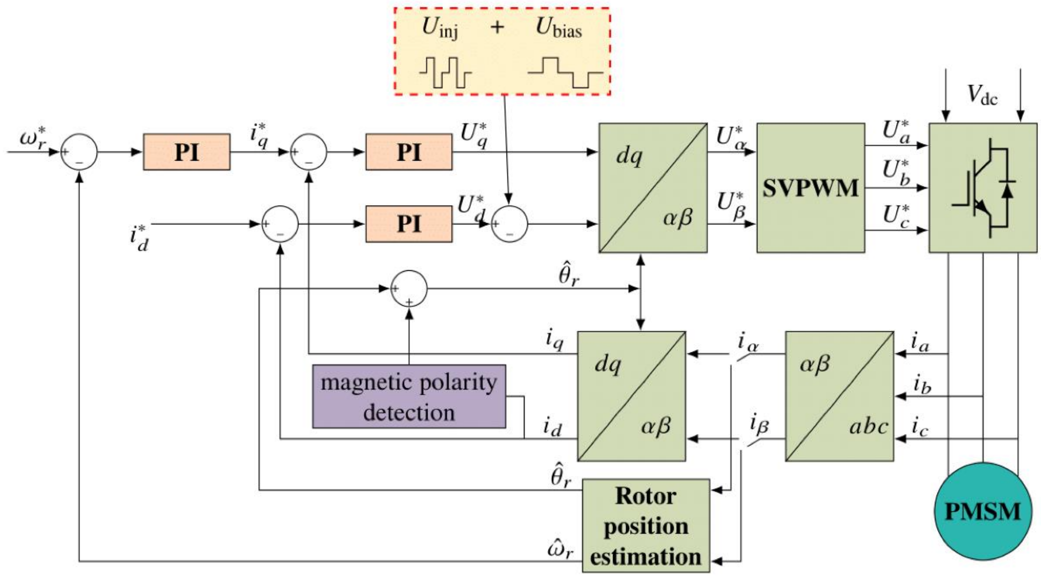

Figure I.11. Functional Block Diagram of the Linear Control Method [2].

1.13.2 Hysteresis Current Control

Hysteresis control for three-phase systems is illustrated in Figure 1.12. It is also known as a nonlinear control technique. In this scheme, the measured currents of the three-phase system are compared with the reference currents, and the resulting error is sent to relays, as shown in Figure 1.12. These relays are also referred to as hysteresis comparators.

These relays are responsible for generating the switching signals for the converter in such a way that the measured values remain within the user-defined hysteresis bandwidth. A low level condition (0) is then produced. The converter output voltage becomes zero, which leads to a decrease in the phase current.

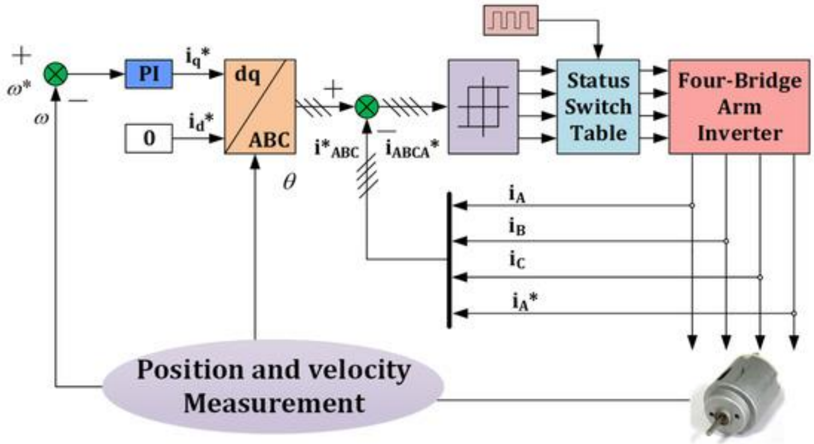

Figure I.12. Hysteresis Current Control Method for PMSMs [2].

1.13.3 Predictive Current Control

Figure 1.13 presents a predictive current control method for motor current regulation. Compared to linear control, this method does not require linear PI controllers or a modulation stage. It provides a different concept and approach for controlling power converters [10–11]. It is a true model-based optimization control method that involves a large number of calculations.

The continuous-time dynamic model of the load current for an RL load with a three-phase two-level inverter is simplified as follows:

The above continuous-time dynamic model of the load current is converted into a discrete-time model, as shown below, for a sampling time.

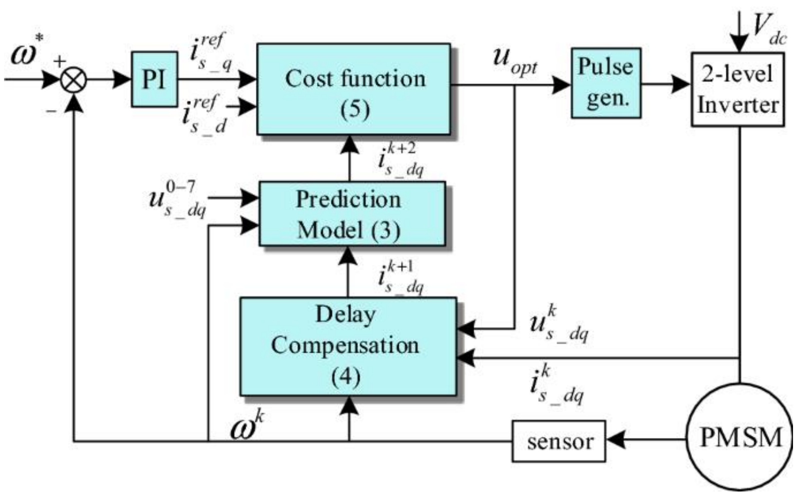

Figure I.13. Functional Block Diagram of Predictive Current Control Method [2].

1.13.4 Deadbeat Predictive Current Control

Figure 1.14 presents a deadbeat-type predictive current control method with a modulation stage. This method is similar to linear PI control, but the PI controller in the linear scheme is replaced by a deadbeat controller.

The deadbeat controller used in this method is responsible for predicting future current behavior at each sampling period, in a similar way to predictive control, using both the load and converter models. It then selects the most appropriate reference voltage vector and applies it to the modulation stage [12,2].

A PWM/SVM modulator is used to generate the switching signals for the power converter, resulting in fixed switching frequency operation.

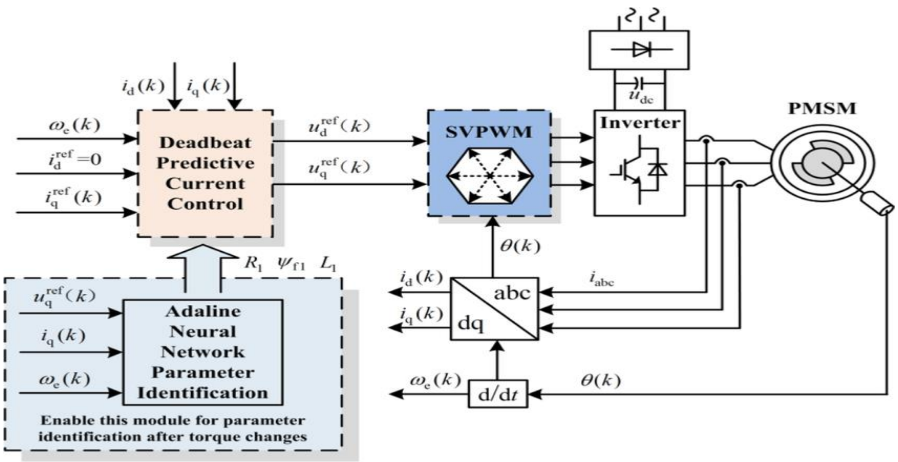

Figure I.14. Functional Block Diagram of Deadbeat Predictive Control Method

1.13.5 Modulated Predictive Control

Figure 1.15 presents the functional block diagram of the modulated predictive control method for motor current regulation. The modulated predictive control method is designed to combine the operating principles of predictive control and SVM [2, 13].

Modulated predictive control performs the cost function optimization in terms of duty cycles, then applies the optimal voltage vectors corresponding to the minimum value of the cost function to the converter through the SVM stage.

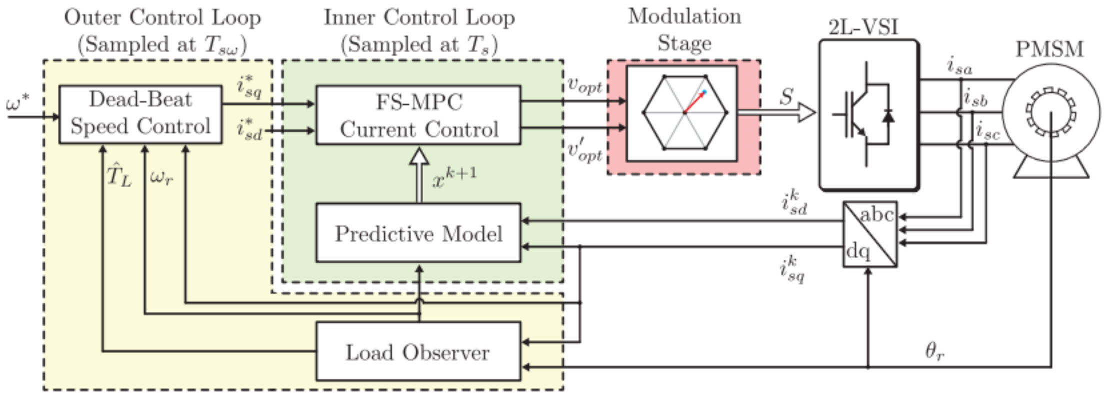

Figure I.15. Functional Block Diagram of Modulated Predictive Control Method [2].

I.13 Conclusion

Permanent magnet synchronous motors (PMSMs) are widely used in industrial applications requiring high performance and high precision, such as electric vehicles (EVs) and automated production systems. Their success is due to several advantages, including high efficiency, high torque and power density, low maintenance requirements, and a high torque-to-inertia ratio.

Thanks to extensive research devoted to their modeling and control, several control strategies have been developed to improve their dynamic performance. Among these, field-oriented control (FOC) is currently one of the most widely used methods for PMSM speed regulation.

The development of power electronic components and the increase in microprocessor computing capabilities have led to the emergence of more advanced control techniques. However, many applications impose strict constraints on current, voltage, torque, and rotational speed to ensure system safety and proper operation. Classical approaches can satisfy these constraints, but often at the cost of degraded dynamic performance.

In this context, model predictive control has attracted increasing interest. This strategy uses a system model to predict future behavior and determine the optimal control action while explicitly taking system constraints into account. Several control architectures have been proposed in the literature for PMSM drives, including partial or full replacement of PI controllers in conventional FOC structures.

Among the most studied approaches are predictive current control, deadbeat predictive control, and modulated predictive control. These methods allow current and voltage constraints to be incorporated in the dq0 rotating reference frame and represent promising alternatives to classical PMSM control strategies.

Chapter II

Modeling and Simulation of a Wind Turbine Based on a Permanent Magnet Synchronous Generator (PMSG).

II.1. Introduction

The increasing use of electrical machines across a wide range of application areas has led to a continuous rise in industrial energy demand. Synchronous-machine-based alternators remain one of the main technologies for electrical energy generation. When coupled with hydraulic, steam, or wind turbines, these systems constitute some of the largest energy conversion units currently in operation.

In permanent magnet synchronous machines (PMSMs), the conventional field winding is replaced by permanent magnets. This configuration eliminates the need for brushes and reduces rotor losses, thereby improving both reliability and efficiency. As a result, PMSMs are widely used in various applications such as machine tools, robotics, aerospace power generation, and electric traction systems.

The analysis and control of these machines are typically based on an accurate mathematical model that includes key electrical parameters such as resistance and inductance. Such models enable a detailed representation of the machine's physical behavior during operation and provide a basis for addressing practical engineering challenges [15].

This chapter first presents the main structural components of the machine, and then develops the mathematical model of the permanent magnet synchronous generator (PMSG) in both the rotor and stator (Park) reference frames. In addition, the operating characteristics of the system under grid-connected conditions are investigated.

II.2 Modeling of the Permanent Magnet Synchronous Generator (PMSG)

II.2.1 Description

An alternator consists of two main parts: a stationary component and a rotating component. The stator, also referred to as the armature, is built from a laminated core that typically has a hollow cylindrical shape. This core contains slots designed to accommodate the conductors of a three-phase winding arranged for 2p poles. The windings are spatially displaced by 2π/32 electrical radians and are generally connected in a star (wye) configuration, with the neutral point often brought out for grounding purposes.

The rotor, which serves as the field system, is composed of p north poles and p south poles arranged alternately. These poles are produced either by field windings supplied with direct current or by permanent magnets. From a structural perspective, rotors are classified as either salient-pole or non-salient (smooth) types, as described in [13].

The number of poles in an alternator is directly related to the rotor speed and the frequency of the generated electrical output. To illustrate this relationship, consider a conductor located in the stator while the rotor's alternating north and south poles pass over it. When a north pole moves past the conductor, the induced voltage follows a positive variation, while the passage of a south pole produces an equal but negative variation. Consequently, each passage of one pole pair corresponds to one complete cycle of the induced voltage waveform. This leads to the well-known relationship between electrical frequency, rotor speed, and number of poles, expressed by the following equation:

$$f = \frac{pn}{120} \qquad \text{(II.1)}$$

II.2.2. Operating Principle of a Synchronous Generator (PMSG)

In a synchronous generator, the mechanically driven rotor field system produces a magnetic field that varies spatially across the stator windings. The electromotive forces (EMFs) induced in these windings give rise to currents, which in turn establish a rotating magnetic field in the air gap. This stator magnetic field rotates at the same speed as the rotor's magnetic field [13].

The fundamental operating principle is based on the interaction between the rotating rotor magnetic field and the stationary stator windings. As the rotor, acting as a magnet, rotates past the three stator coils connected to the electrical network, it causes a time-varying magnetic flux in each coil. This variation in flux induces an electromotive force in each phase winding, resulting in the generation of a balanced three-phase current.

II.2.3. Modeling of the Permanent Magnet Synchronous Generator

Similar to other three-phase electrical machines, this generator is equipped with a wound stator. However, a key distinguishing feature of the Permanent Magnet Synchronous Generator (PMSG) is the use of permanent magnets in the rotor. This configuration eliminates the need for brushes and slip rings, thereby reducing rotor losses and removing the requirement for an external excitation current supply [18]. As a result, an electromotive force is induced in each stator winding, producing a three-phase output current.

The modeling of a Permanent Magnet Synchronous Generator (PMSG) relies on the development of a rigorous mathematical framework. Such a model is necessary to accurately describe the electromagnetic and mechanical processes governing the machine's operation. It enables a detailed analysis of the system state variables under both transient and steady-state conditions, providing a solid basis for simulation and performance evaluation [19].

II.2.5 Electrical Equations of the PMSG:

The electrical equations of electrical machines in a stationary reference frame linked to the stator are described by:

$$\begin{bmatrix} V_a \\ V_b \\ V_C \end{bmatrix} = [-R_s] \begin{bmatrix} i_a \\ i_b \\ i_c \end{bmatrix} + \frac{d}{dt} \begin{bmatrix} \varphi_a \\ \varphi_b \\ \varphi_c \end{bmatrix} \quad \text{(II.2)}$$

$(V_a V_b V_c)$: Stator phase voltage vector.

$(i_a i_b i_c)$: Stator phase current vector.

$(\varphi_a \varphi_b \varphi_c)$: Vector of the total flux linkages through the stator windings.

R_s : Stator phase resistance.

The stator windings of the synchronous machine under consideration are connected in a star (wye) configuration with an isolated neutral point. This arrangement ensures that the instantaneous sum of the stator phase currents is always zero, thereby eliminating the presence of zero-sequence currents. As a result, even if zero-sequence components of voltage or flux exist in the system, they do not contribute to the electromagnetic torque production.

II.2.6 Transformation to the Park Reference Frame

To simplify the dynamic model of the machine, a reference frame transformation is employed. This mathematical operation effectively maps the three fixed stator windings, originally displaced

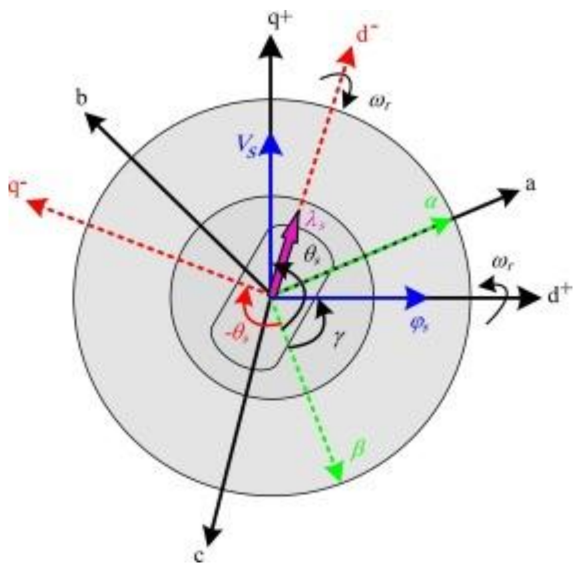

Figure II.1. Representation of (PMSG) in the Park (d, q) Reference Frame.

by (2π/3), onto a new representation comprising two fictitious equivalent windings. These transformed windings exhibit a (π/2) phase shift and are inherently aligned with the rotor's reference frame

The two d- and q-axis coils, rotating synchronously with the rotor, generate an effect comparable to that produced by the three stationary windings. Expressing system variations within this newly established (d, q) reference frame facilitates the transformation from the natural

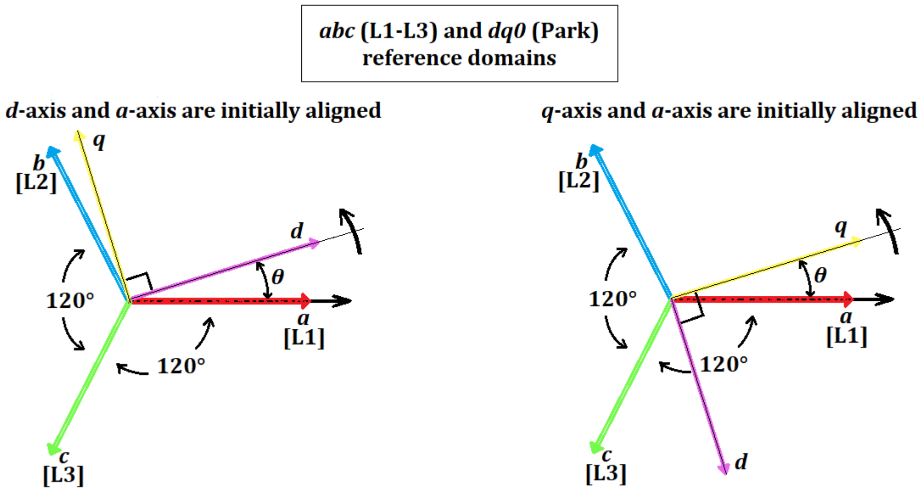

Figure II.2. Transformation from the Stator Natural Reference Frame to the Park (d,q) Reference Frame.

coordinate system to the Park reference frame, thereby yielding a relatively simplified model of the machine [17].

Using the Park transformation, the real (phase) quantities (v_a, v_b, v_c) and (i_a, i_b, i_c) are transformed into their components in the new reference frame (v_0, v_b, v_c) and (i_0, i_b, i_c).

The Park transformation matrix is expressed as follows:

$$P(\theta) = \begin{bmatrix} cos(\theta) & cos\left(\theta - \frac{2\pi}{3}\right) & cos\left(\theta - \frac{4\pi}{3}\right) \\ -sin(\theta) & -sin\left(\theta - \frac{2\pi}{3}\right) & -sin\left(\theta - \frac{4\pi}{3}\right) \\ \frac{1}{2} & \frac{1}{2} & \frac{1}{2} \end{bmatrix} \quad \text{(II.3)}$$

The inverse Park transformation is given by:

$$P^{-1}(\theta) = \begin{bmatrix} cos(\theta) & -sin(\theta) & 1 \\ cos\left(\theta - \frac{2\pi}{3}\right) & -sin\left(\theta - \frac{2\pi}{3}\right) & 1 \\ cos\left(\theta - \frac{4\pi}{3}\right) & -sin\left(\theta - \frac{4\pi}{3}\right) & 1 \end{bmatrix} \quad \text{(II.4)}$$

II.2.7 Magnetic Equations

In synchronous machines with a sinusoidal distribution of conductors, (φ_d) and (φ_q) are linear functions of the currents (i_d) and (i_q):

$$\varphi_d = L_d i_d + \varphi_f \quad \text{(II.5)}$$
$$\varphi_q = L_q i_q \quad \text{(II.6)}$$

L_d and L_q are the direct-axis and quadrature-axis inductances, respectively, and they are assumed to be independent of θ .

φ_f represents the magnetic flux produced by the permanent magnets.

By adopting the generator convention, the directions of the currents i_d and i_q are reversed within the park reference. Consequently, the derived model for the permanent magnet synchronous generator can be formulated as:

$$V_d = R_s I_d - L_d \frac{dI_d}{dt} + \omega L_q I_q \quad \text{(II.7)}$$

$$V_q = R_s I_q - L_q \frac{dI_q}{dt} - \omega L_d I_d + \omega \varphi_f \quad \text{(II.8)}$$

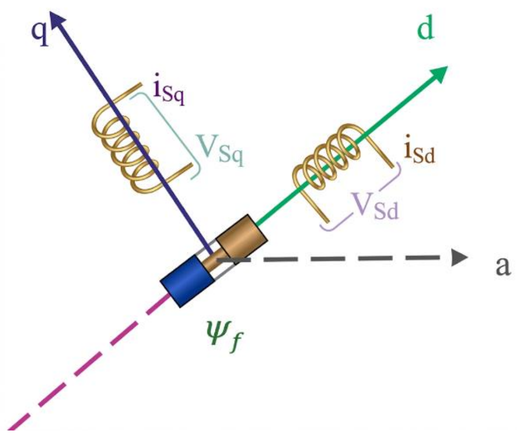

II.2.8 Expression of the Electromagnetic Torque

The electromagnetic torque (C_{em}) is conventionally expressed as the partial derivative of the electromagnetic energy stored with respect to the rotor's mechanical angular position [17]:

$$C_{em} = \frac{dW_e}{d\theta_{geo}} = P \frac{dW_e}{d\theta_e} \quad \text{(II.9)}$$

W_e: Energy stored in the magnetic circuit.

θ_{geo}: Angular displacement of the moving part.

P: Number of pole pairs.

The expression of the power transmitted in the Park reference frame is given by:

$$P(t) = \frac{3}{2}\left(V_d I_d + V_q I_q\right) \quad \text{(II.10)}$$

By substituting V_d and V_q with their respective expressions, we obtain:

$$P(t) = \frac{3}{2}\left[-R_s\left(i_d^2 + i_q^2\right) + \frac{d}{dt}\left(\varphi_d i_d + \varphi_q i_q\right) + \omega\left(\varphi_d i_q - \varphi_q i_d\right)\right] \quad \text{(II.11)}$$

$\frac{3}{2} R_s\left(i_d^2 + i_q^2\right)$: Represents the power dissipated as Joule losses in the stator windings

$\frac{3}{2}\left(\varphi_d \frac{di_d}{dt} + \varphi_q \frac{di_q}{dt}\right)$: Represents the variation of the magnetic energy stored in the stator windings

$\frac{3}{2}\left(\varphi_d i_q - \varphi_q i_d\right)\frac{d\theta}{dt}$: Represents the electromagnetic power. Knowing that:

$$\omega = p\,\Omega \quad \text{and} \quad P_{em} = C_{em}\,\Omega \quad \text{(II.12)}$$

The expression of the electromagnetic torque can be written as:

$$C_{em} = \frac{3}{2} p\left(\varphi_d i_q - \varphi_q i_d\right) \quad \text{(II.13)}$$

After performing the necessary substitutions, it can be expressed as :

$$C_{em} = \frac{3}{2} p\left[\left(L_d - L_q\right) i_d i_q + \varphi_f i_q\right] \quad \text{(II.14)}$$

II.2.9 Mechanical Equations

The dynamic equation of the PMSG is given as follows:

$$J\frac{d\Omega}{dt} = C_m - C_{em} - f\Omega \quad (II\text{-}13) \quad \text{(II.15)}$$

Where:

- $\boldsymbol{T_m}$: Mechanical torque applied to the generator
- $\boldsymbol{T_{em}}$: Electromagnetic torque
- $\boldsymbol{f\Omega}$: Friction torque
- $\boldsymbol{J}$: Total moment of inertia of the machine
- $\boldsymbol{f}$: Viscous friction coefficient

II.3 Turbine Modeling:

II.3.1 Aerodynamic Torque of the Wind Turbine:

Turbine modeling requires the development of an accurate mathematical representation that describes the power extracted from the wind as a function of both the incoming wind speed and the turbine operating conditions, particularly its rotational speed. This approach aims to improve the understanding of the turbine's dynamic behavior under different operating scenarios and to enable the evaluation of overall system performance.

In addition, such a model allows the aerodynamic torque acting on the low-speed shaft of the wind turbine to be quantified, which is essential for analyzing the energy conversion process within the system. Consequently, the available wind power, also referred to as aerodynamic power, is defined as follows: [1–2].

$$P_v = \frac{1}{2}\rho S V^3 = \frac{1}{2}\rho.\pi.R^2.V^3 \quad \text{(II.16)}$$

ρ: Air density, equal to 1.22 kg/m³ at atmospheric pressure and 15°C. According to Betz's law, this power can never be fully extracted.

S: The circular area swept by the turbine; the radius of the circle is determined by the blade length R, where $S = \pi R^2$.

V: Wind speed.

In reality, the conversion device (the wind turbine) extracts an aerodynamic power $P_t$that is lower than the available power P_v.

$$P_t = \frac{1}{2} C_p(\lambda, \beta)\rho\, \pi\, R^2\, V^3 \quad \text{(II.17)}$$

A wind turbine can only convert a certain percentage of the power captured from the wind. This percentage is represented by $C_p(\lambda, \beta)$, which depends on the tip-speed ratio $\lambda$and the blade pitch angle β.

The power coefficient $C_p$represents the aerodynamic efficiency of the wind turbine (P_t/P_v). It depends on the turbine's characteristics. The expression of the power coefficient is interpolated in the following form:

$$C_p(\lambda, \beta) = A_1\left(\frac{A_2}{\lambda_i} - A_3\beta - A_4\right)e^{-\frac{A_5}{\lambda_i}} + A_6\lambda \quad \text{(II.18)}$$

With:

$$\frac{1}{\lambda_i} = \left(\frac{1}{\lambda + 0.08\beta} - \frac{0.035}{\beta^3 + 1}\right) \tag{II.19}$$

presents the observed variation of the power coefficient (C_p) for the wind turbine examined in this thesis. The maximum power coefficient (C_{pmax}) of 0.48 is achieved when the blade pitch angle (β) is 0° and the tip-speed ratio attains its optimal value (λ_{optim}) of 8.1. To optimize power extraction, it is imperative to operate the turbine at this specific optimal tip-speed ratio, thus sustaining the power coefficient at its peak value (C_{pmax} = 0.48).

The turbine torque is defined as the ratio of the aerodynamic power to the turbine's rotational speed, (Ω_t).

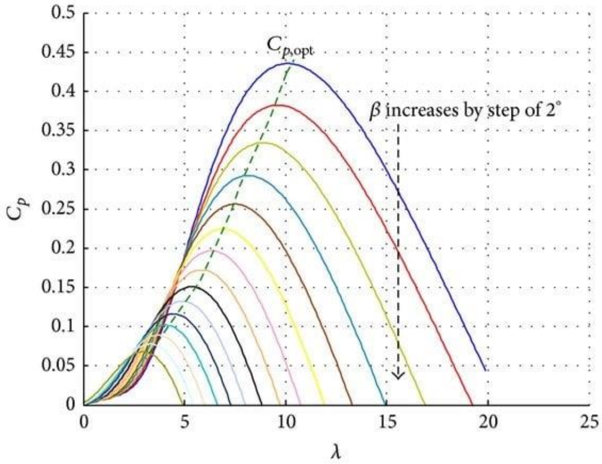

Figure II.3. Variation of the Power Coefficient as a Function of λ and β.

$$T_t = \frac{1}{2}\frac{\rho\pi R^2 C_p(\lambda,\beta)V^3}{\Omega_t} \tag{II.20}$$

with $\boldsymbol{\omega_t} = \boldsymbol{\omega_m}$ since the gearbox ratio k = 1

Ω_t : Turbine speed.

T_t : Aerodynamic torque.

The tip-speed ratio (λ) is defined as the ratio between the linear speed of the blades (i.e., the turbine's rotational speed) and the wind speed.

$$\lambda = \frac{\Omega_t R}{V} \tag{II.21}$$

As depicted in (Figure 2.1), the power coefficient typically achieves its peak at a particular tip-speed ratio, referred to as (λ_{opt}). At this specific operational state, the power coefficient (C_p) reaches its highest point, which is indicative of the most efficient power capture from the available wind resource.[29]

Based on this fundamental principle, it is possible to develop control strategies that ensure optimal power extraction over a wide range of wind speeds. This operating mode is maintained until the generator reaches its rated power. Beyond this point, any additional available wind power is limited, and the output is constrained to the nominal rated value [2].

II.3.2 Power Maximization and Pitch Angle Control

The formulation of the control strategy is based on the assumption that wind speed variations remain negligible during steady-state operation. Under this assumption, the aerodynamic torque can be accurately estimated by combining the available wind speed estimate with the measured mechanical rotational speed of the turbine.

$$T_t^* = \frac{P_{tmax}}{\omega_m^*} = \frac{1}{2\omega_m^*} C_{Pmax} \rho S V_{ref}^3 \quad \text{(II.22)}$$

Given the inherent challenges in directly measuring wind speed at the turbine level, its value is typically estimated through the application of the subsequent equation.

$$V_{ref} = \frac{\omega_m^* R}{\lambda_{opt}} \quad \text{(II.23)}$$

Additionally, to safeguard the wind energy system and ensure its stable operation, while simultaneously maintaining power output at its nominal level, pitch angle control is a frequently adopted mechanical strategy. This approach involves modifying the blade pitch angle in response to variations in wind speed. Its primary function is to regulate both the output power and rotational speed when the generator speed surpasses 30% of its rated capacity. [1].

II.4 Modeling of Inverter

The two-level three-phase inverter is one of the most widely used topologies for connecting decentralized generation systems to the electrical grid. It enables the conversion of a DC input voltage Vdc into a three-phase AC output through PWM control, which regulates the switching duty cycles of semiconductor devices such as IGBTs or MOSFETs [12].

Each inverter leg can switch between two voltage levels, either $+V_{dc}/2$ or $-V_{dc}/2$, depending on the adopted configuration (with or without a neutral point).

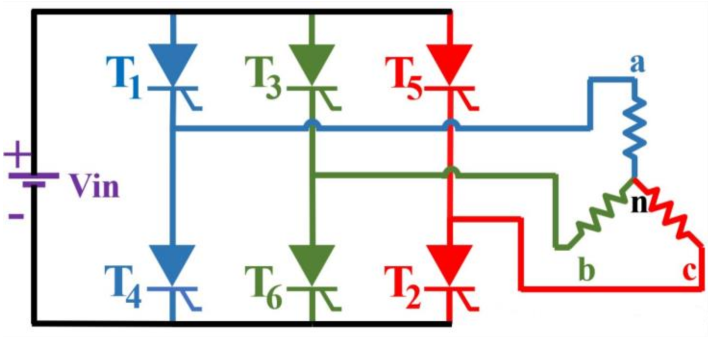

Figure II.4. Schematic Diagram of an Inverter.

The line voltages at the inverter terminals are expressed as follows:

$$\begin{cases} U_{ab} = V_{ao} + V_{bo} = V_{ao} - V_{bo} \\ U_{bc} = V_{bo} + V_{co} = V_{bo} - V_{co} \\ U_{ca} = V_{co} + V_{ao} = V_{co} - V_{ao} \end{cases} \quad \text{(II.24)}$$

U_{ab}, U_{bc}, and U_{ca} can be considered as the inverter input voltages.

The inverter equation in matrix form is represented as follows:

$$\begin{bmatrix} V_{an} \\ V_{bn} \\ V_{cn} \end{bmatrix} = \frac{u_0}{3} \begin{bmatrix} 2 & -1 & -1 \\ -1 & 2 & -1 \\ -1 & -1 & 2 \end{bmatrix} \begin{bmatrix} S_a \\ S_b \\ S_c \end{bmatrix} \quad \text{(II.25)}$$

II.5 Modeling of Rectifier

The machine-side converter constitutes a key component in the energy conversion chain of a wind energy system based on a permanent magnet synchronous generator (PMSG). It acts as the interface between the generator and the DC link, ensuring the controlled transfer of the electrical energy generated by the turbine to the grid-side conversion stage.

In modern high-performance wind energy systems, a PWM rectifier combined with a filtered DC bus is commonly employed to facilitate bidirectional power flow control and enhance the quality of the exchanged energy [12].

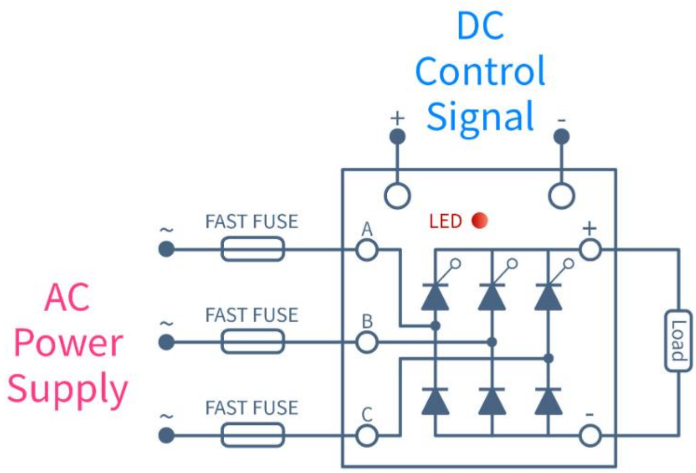

Figure II.5. Schematic Diagram of a Rectifier.

On peut simplifier la modélisation et diminuer le temps de simulation en représentant le redresseur par un ensemble d'interrupteurs idéaux. Ces interrupteurs sont complémentaires, et leur état est déterminé par la fonction suivante :

$$S = \begin{cases} +1, & \overline{S} = -1 \\ -1, & \overline{S} = +1 \end{cases} \quad \text{pour } S = a, b, c \tag{II.26}$$

Puis, les tensions de phase d'entrée et le courant de sortie peuvent être écrits en fonction de :

$$i_a + i_b + i_c = 0 \tag{II.27}$$

Les tensions d'entrée entre phases du redresseur MLI peuvent être décrites par :

$$\begin{cases} U_{sab} = (S_a - S_b)V_{dc} \\ U_{sbc} = (S_b - S_c)V_{dc} \\ U_{sca} = (S_c - S_a)V_{dc} \end{cases} \tag{II.28}$$

II.7. Conclusion

This chapter presented the mathematical and operational modeling of the Permanent Magnet Synchronous Generator (PMSG), including the fundamental electrical and mechanical equations that describe its behavior. The Park transformation was introduced as an effective tool for simplifying the machine model and facilitating its analysis and control. In addition, the main control principles and techniques required to evaluate system performance and enhance operational stability were discussed.

The chapter also examined the wind turbine model and the associated power conversion stages, including the rectifier, the DC-link, and the inverter. These components play a crucial role in the efficient conversion and transfer of energy from the wind turbine to the electrical grid.

Overall, the developed models provide a comprehensive framework for understanding the dynamic behavior of the wind energy conversion system. They establish the theoretical foundation necessary for the design, implementation, and evaluation of advanced control strategies, which

Chapter III

Proposed Predictive Current Control Strategy Based on the GWO Algorithm

III.1 Introduction:

Permanent Magnet Synchronous Motors (PMSMs) require advanced control strategies to achieve high-performance operation and accurate current regulation. Model Predictive Control (MPC) offers excellent dynamic response and constraint-handling capabilities; however, its effectiveness depends heavily on the proper tuning of control parameters. To enhance controller performance, the Grey Wolf Optimizer (GWO) is integrated with the predictive control framework to determine optimal parameter values. This section presents the proposed GWO-based predictive current control strategy and outlines its implementation through the corresponding algorithm flowchart.

III.2 Predictive Current Control of PMSMs

III.2.1 General Overview of Predictive Current Control

Classical predictive control, which is a branch of model predictive control, can be described as a new control strategy based on the system model, including both the converter and the machine, to predict its future behavior over a prediction horizon based on a user-defined optimal criterion, ultimately generating the optimal system behavior.

More specifically, the classical predictive control model predicts the behavior of the controlled variables, i.e., the machine current, for each possible finite switching state generated by the converter. Thus, to select the appropriate switching state to be applied, selection criteria must be defined.

This criterion consists of a cost function that is evaluated using the predicted current values, thereby measuring the error between the reference current and the predicted current. The current is computed (i.e., predicted) for each possible switching state of the converter, and the state that minimizes the cost function is selected, ensuring that the error between the measured stator current and its reference value is small.

Therefore, the general principle of the control algorithm mainly consists of three key elements:

- The dynamic mathematical model of the drive system (converter and machine).
- A user-defined criterion, i.e., a cost function, which ultimately determines the system behavior through a sequence of control actions over a prediction horizon N.
- The optimization of the cost function, where only the optimal control action from the generated sequence is applied, while the others are discarded. The control algorithm is then repeated at the next sampling period.

The general operating principle of predictive control is illustrated in more detail in Figure 3.1, where, at the sampling instant Ts (in the ideal case), system measurements and predicted control actions are performed. Control actions are obtained by minimizing a cost function that evaluates the best future control action to be taken.

The optimal control action is then implemented, and system variables are measured and recalculated in the next sampling period based on the system state at that time, generating new control actions with a shifted prediction horizon.

However, for real-time discrete applications, a longer step horizon must be introduced due to the impossibility of simultaneously performing system measurements and computing control actions. Thus, a two-step prediction horizon is often used [7–8].

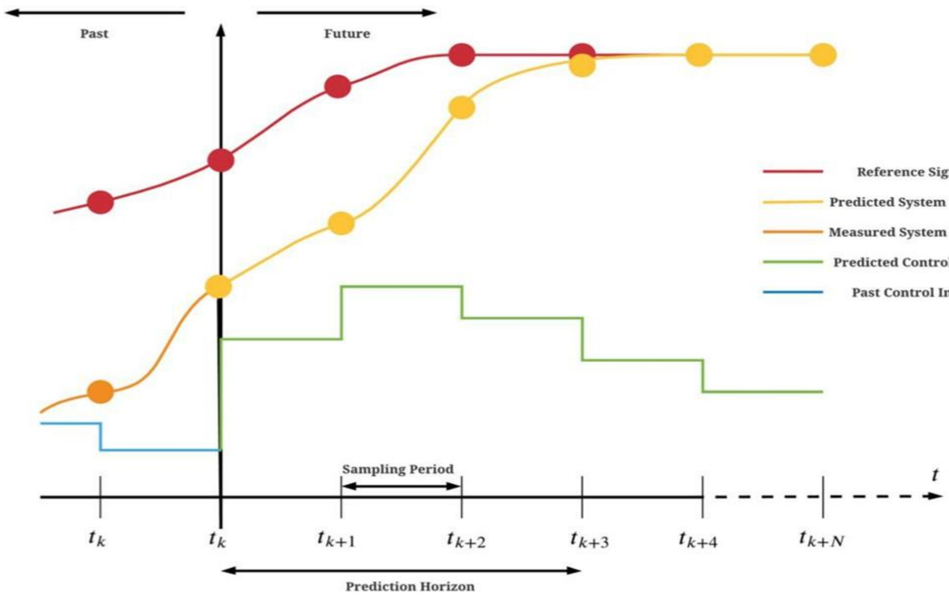

Figure III.1. Block Diagram of Predictive Current Control.

predictive current control efficiently handles complex dynamic systems subject to variations and allows the integration of multiple constraints and nonlinearities within the control system, making it a versatile control technique. These characteristics are inherent in industrial processes and real systems, thereby posing a challenge to classical control techniques, which are better suited to less complex systems.

Moreover, a key difference from traditional optimal control lies in the use of a cost function to globally evaluate system performance over a prediction horizon, enabling the optimization of control variables, i.e., the current. In addition, the predicted current output is based on previous system information as well as possible predicted current values within the moving horizon, highlighting the role of the system model.

In particular, in predictive current control, the optimal predicted current values are not obtained by evaluating the error between the reference and feedback signals, as in a classical PID controller. Instead, they are obtained by minimizing the cost function used as a performance function, i.e., penalizing future control actions, where only the optimal solution is selected and applied over the prediction horizon. Furthermore, predictive current control is implemented as a digital control strategy.

Nevertheless, due to the high flexibility of the optimization problem, where various constraints and objectives can be added to the cost function, as well as the chosen prediction horizon N to improve control performance, the trade-off generally lies in the high computational cost of predictive current control.

Several solutions to overcome this issue and its drawbacks were presented in Chapter 1. In the following section, another solution is proposed.

III.2.2 Two-Level Three-Phase Inverter

In this work, the considered drive system configuration consists of a two-level three-phase inverter connected to the PMSM. The inverter is characterized by six IGBTs (from T1 to T6) and their respective antiparallel diodes, where the control system generates the optimal voltage vector through a combination of switching signals S_a, S_b, and S_c.

In addition, a closed-loop scheme with measurement sensors is considered, in which the rotor position, stator currents, and DC-link voltage Vdc are measured to ensure high drive efficiency. The configuration of the PMSM drive system is illustrated in Figure 3.2.

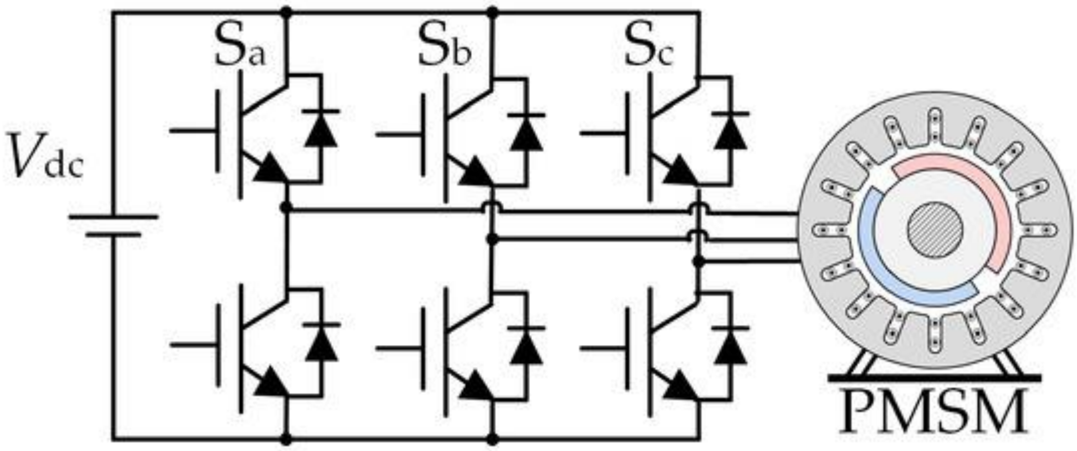

Figure III.2. Configuration of the PMSM Drive System with a Two-Level Three-Phase Inverter

A more detailed analysis of the inverter allows us to deduce the following mode of operation for a given phase as an example:

- If Switch ON; then Switch OFF; So, T_1T_2: $S_a = 1, S'_a = 0$
- If Switch then Switch then, T_1: **OFF**; T_2: **ON**; $S_a = 0, S'_a = 1$

This is true for the phases and. Therefore, the relationship between the phase output voltage (line-neutral) and the switching states of the inverter is given by:

$$\begin{bmatrix} v_a \\ v_b \\ v_c \end{bmatrix} = \frac{V_{dc}}{3}\begin{bmatrix} 2 & -1 & -1 \\ -1 & 2 & -1 \\ -1 & -1 & 2 \end{bmatrix}\begin{bmatrix} S_a \\ S_b \\ S_c \end{bmatrix} \tag{III.1}$$

Since for each of the three phases, there are two control actions defined by the switch's ON-OFF activity, the representation of the voltage vector of the phase voltages corresponding to the eight different switching states/combinations that can be generated by the inverter can be calculated using the definition of the spatial vector where there are switching states, the spatial vector of the voltage being defined as follows:$2^3 = 8$

$$v_s = \frac{2}{3}V_{dc}(v_a + av_b + a^2v_c) \qquad (III.2)$$

Where the rotation factor of space is given by . The output voltage of the inverter in an equivalent in a stationary reference frame can be obtained by using the following transform:$a = e^{j2\pi/3}\alpha\beta$

$$\begin{bmatrix} v_\alpha \\ v_\beta \end{bmatrix} = \frac{2}{3}\begin{bmatrix} 1 & -\frac{1}{2} & -\frac{1}{2} \\ 0 & \frac{\sqrt{3}}{2} & -\frac{\sqrt{3}}{2} \end{bmatrix}\begin{bmatrix} x_a \\ x_b \\ x_c \end{bmatrix} \qquad (III.3)$$

Therefore, using (3.1) in (3.3), the output voltage vectors of the inverter in the coordinate system are given by:

$$\begin{cases} v_\alpha = \frac{2}{3}V_{dc}\left(S_a - \frac{S_b + S_c}{2}\right) \\ v_\beta = \frac{1}{\sqrt{3}}V_{dc}(S_b - S_c) \end{cases} \qquad (III.4)$$

The evaluation of (3.4) for the different switching states gives the spatial vector at eight voltages generated by the inverter, as shown in Table 3.1, which details the relationship between the output voltages and the eight conductive modes, i.e., the switching states of the

The three-phase inverter with 2 levels are given in Table 3.1 where . In addition, it can be observed that the generated vectors are categorized into six active voltage vectors (to $V_j(j = 0, \dots, 7)V_1V_6$) and two null (inactive) voltage vectors ($V_0$and V_7). In addition, the hexagonal voltage vector can be seen in Figure 3.3, where the six active voltage vectors define the axes of the hexagon of the voltage vector and the voltage vectors that are zero at the origin, with an angle between two adjacent active vectors of 60 degrees. The relationship between the output voltages and the eight conduction modes, i.e. the switching states of the three-phase inverter, is given in Table 3.1 where $S_j(j = 0, \dots, 7)$

It should be noted that due to the existence of the two zero voltage vectors as shown in Table 3.1, multiple switching combinations, multiple switching combinations can be generated. Nevertheless, in real-world applications, it is common to choose one or the other in order to reduce the complexity of implementing predictive control [10-11]. So, in this work, V_0 is chosen as a zero vector.

III.2.3 Predictive Current Control Applied to MSAPs

For the numerical implementation of predictive current control, a discretization method is necessary to approximate its continuous case. Given the short sampling time ( ) used in this work, the explicit Euler discretization method is considered the most appropriate because of its simplicity, and is expressed as follows:T_s

$$\frac{di(t)}{dt} = \frac{i[k+1] - i[k]}{T_s} \qquad (III.5)$$

Table 3.1. Voltage vectors at the output of a three-phase 2-stage inverter.

$V_j(S_a, S_b, S_c))$	v_a	v_b	v_c
$V_0(0,0,0)$	0	0	0
$V_1(1,0,0)$	$2/3v_{dc}$	$-1/3v_{dc}$	$-1/3v_{dc}$
$V_2(1,1,0)$	$1/3v_{dc}$	$1/3v_{dc}$	$-2/3v_{dc}$
$V_3(0,1,0)$	$(-1/3v_{dc})$	$(2/3v_{dc})$	$(-1/3v_{dc})$
$V_4(0,1,1)$	$-2/3v_{dc}$	$1/3v_{dc}$	$1/3v_{dc}$
$V_5(0,0,1)$	$-1/3v_{dc}$	$-1/3v_{dc}$	$2/3v_{dc}$
$V_6(1,0,1)$	$1/3v_{dc}$	$-2/3v_{dc}$	$(1/3v_{dc})$
$V_7(1,1,1)$	0	0	0

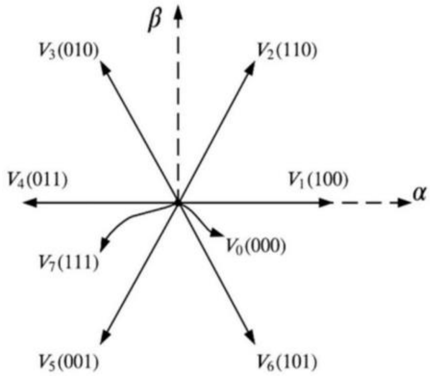

Figure III.3. Hexagonal representation of the voltage vectors of a three-phase 2-stage inverter.

Initially, the equivalent stator voltage is reconstructed using the optimal voltage vector as seen in (3.1) in the reference frame (dq) using (2.1). Therefore, considering the direct Euler discretization method (used throughout this work), the discrete-time version equations corresponding to (2.10) can be stated as:

$$\begin{cases} v_{ds}^k = R_s i_{ds}^k - \omega_r L_{qs} i_{qs}^k + \frac{L_{ds}}{T_s}\left(i_d^{k+1} - i_d^k\right) \\ v_{qs}^k = R_s i_{qs}^k - \omega_r L_{ds} i_{ds}^k + \frac{L_{ds}}{T_s}\left(i_q^{k+1} - i_q^k\right) + \omega_r \psi_r \end{cases} \quad \text{(III.6)}$$

Where is the sampling interval, $T_s i_{ds}^k$ and i_{qs}^k are the currents measured at the ends of the direct and quadrature axes at the instant, and kv_{ds}^k and v_{qs}^k are the direct and quadrature axis voltages obtained from the optimal voltage vector applied to the inverter at the time. Thus, up to (3.6), the stator currents predicted in the sampling period are given by:$kk + 1$

$$\begin{cases} i_{ds}^{k+1} = \left(1 - \dfrac{R_s T_s}{L_{ds}}\right) i_{ds}^{k} + \omega_r T_s \dfrac{L_{qs}}{L_{ds}} i_q^k + \dfrac{T_s}{L_{ds}} v_{ds}^k \\ i_{qs}^{k+1} = \left(1 - \dfrac{R_s T_s}{L_{qs}}\right) i_{qs}^{k} - \omega_r T_s \dfrac{L_{ds}}{L_{qs}} i_{ds}^k + \dfrac{T_s}{L_{qs}} v_{qs}^k \end{cases} \tag{III.7}$$

Using predictive current control with delay compensation from [54] and according to (3.7), the predicted currents in the sampling period th can be written as: $(k+2)$

$$\begin{cases} i_{ds}^{k+2} = \left(1 - \dfrac{R_s T_s}{L_{ds}}\right) i_{ds}^{k+1} + \omega_e T_s \dfrac{L_{qs}}{L_{ds}} i_{qs}^{k+1} + \dfrac{T_s}{L_{ds}} v_{ds}^{k+1} \\ i_{qs}^{k+2} = \left(1 - \dfrac{R_s T_s}{L_{qs}}\right) i_{qs}^{k+1} - \omega_e T_s \dfrac{L_{ds}}{L_{qs}} i_{ds}^{k+1} + \dfrac{T_s}{L_{qs}} v_{qs}^{k+1} \end{cases} \tag{III.8}$$

Where v_{ds}^{k+1} and v_{qs}^{k+1} are reconstructed from the 8 vectors of the hexagonal voltage that the converter can synthesize. Next, the cost function is defined with a focus on the desired behavior of the MSAP. Therefore, since the implemented algorithm focuses on the predictive currents, the cost function is then defined to evaluate the error between the predicted currents and their respective baselines. Thus, the cost function is given by:

$$g(k)|_{x_i} = \left[i_{ds}^* - i_{ds}^{k+2}\right]^2 + \left[i_{qs}^* - i_{qs}^{k+2}\right]^2; i = 0, \dots, 7 \tag{III.9}$$

In the MSAP control, a speed control loop with an integral proportional controller (PI) generates the "control signal" from the error (difference) between the desired mechanical reference speed and the actual measured mechanical speed emitted by the machine in order to correctly follow the reference speed, as shown in Figure 3.3. Since the PI speed controller used uses closed-loop control feedback, a speed sensor is also used to track the actual speed of the machine and get the rotor location. In addition, the performance of the PI cruise control is highly dependent on its parameterization (controller gains), with the proportional component being responsible for proportionally adjusting the control signal to an existing error, The values assigned to the PI cruise control gains are given in Appendix A. Hence the "control signal", i.e. the reference current to the asterisk operator power generated by the speed controller PI, while to the asterisk operator power is derived from the examination of the maximum torque per ampere strategy in , given by: $K_p i_{qs}^* i_{ds}^*$ [7,16]

$$i_{ds}^* = -0.0589 i_{qs}^2 + 1.0515 i_{qs} - 0.2374 \tag{III.10}$$

Therefore, by optimizing (3.9), the optimal voltage vector can be determined as follows:

$$V_{VSI}(k) = \arg \min_{(x_0, \dots, x_7)} g(k)\Big|_{x_i}, i = 0, \dots, 7 \tag{III.11}$$

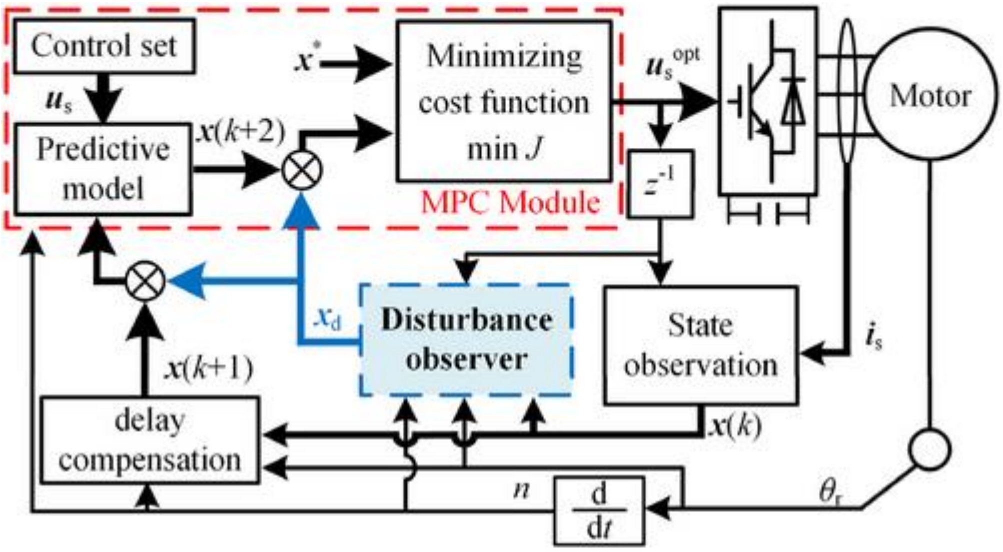

Figure III.4. Conventional predictive control of the MSAP [10].

III.3 Advanced Predictive Control of MSAP Current

The classical predictive control of the current is based on the MSAP model, the current prediction depends mainly on the accuracy of the parameter. In fact, obtaining precise values of MSAP parameters is impossible [13,14]. Therefore, in order to avoid the effects of parameter inconsistencies, a new advanced predictive current control is proposed, which relies on a Grey Wolf Optimizer (GWO) to follow the minimum cost function, thus benefiting from the following advantages: high accuracy of the solution, fast convergence, low tuning and computational efforts, and the ability to handle the local optimum [16].

III.3.1 Advanced Predictive Control of MSAP Current Proposed

In the case of classical predictive control, the expression (3.8) can be simplified by omitting the terms, assuming that the sampling time is very short [16]. On the other hand, when an optimal input factor is imposed, as in (3.12), the second term in (3.8) has no effect on the choice of the optimum voltage vector among the eight possible vectors and can therefore be ignored. In (3.12), a discrete model with no machine parameters is represented using the simplified expression of (3), with the aim of developing a model unrelated to any machine model and parameter, defined as:$R_sT_s/L_{sdq}X_{opt} = 1/L_{sdq}$

$$\begin{cases} i_{ds}^{k+1} = X_{\text{opt}}\, T_s v_{ds}^k + i_{ds}^k \\ i_{qs}^{k+1} = X_{\text{opt}}\, T_s v_{qs}^k + i_{qs}^k \end{cases} \tag{III.12}$$

Where denotes the optimal input factor. The search for the optimal value for is based on the GWO, which can ensure an appropriate current prediction. Similar to (4), the dq-axis currents must be predicted at the parenthesis the of the sampling period, using the following expression:$X_{opt}X_{opt}k + 2$

$$\begin{cases} i_{ds}^{k+2} = X_{opt}T_s v_{ds}^{k+1} + i_{ds}^{k+1} \\ i_{qs}^{k+2} = X_{opt}T_s v_{qs}^{k+1} + i_{qs}^{k+1} \end{cases} \tag{III.13}$$

Unlike the classic predictive control using (3.6)-(3.8), the advanced predictive control offered in (3.12) and (3.12) does not use any machine models or parameters. Next, the proposed advanced predictive control optimal voltage vector is selected by evaluating and minimizing the cost function as in (3.9) and (3.11), respectively, and considering the maximum torque per ampere strategy defined in (3.10), in a manner similar to the classical predictive control.

III.2 Optimization Methods

III.2.1 presentation:

Numerous optimization problems are characterized by high complexity and the absence of exact analytical solutions, leading to the emergence of metaheuristic optimization techniques inspired by natural phenomena. These algorithms emulate the collective behavior of living organisms to efficiently search for optimal or near-optimal solutions in large and complex search spaces. Optimization methods are generally classified into deterministic and stochastic approaches, with stochastic algorithms offering superior capability to escape local optima through randomization and global exploration mechanisms.

Among the most widely adopted metaheuristic techniques are Genetic Algorithms (GA), Ant Colony Optimization (ACO), and Particle Swarm Optimization (PSO). More recently, the Grey Wolf Optimizer (GWO), inspired by the social hierarchy and cooperative hunting strategy of grey wolves, has attracted considerable interest. Owing to its simplicity, effective balance between exploration and exploitation, and fast convergence characteristics, GWO has demonstrated competitive performance in various applications, including automatic control, economic dispatch, feature selection, and multi-objective optimization problems. [22].

III.2.2 Principle of operation

Optimization plays a fundamental role in almost every field, ranging from engineering design and economic planning to transportation, logistics, and communication networks. Because resources such as time, energy, and cost are inherently limited, achieving their most efficient utilization is of paramount importance. Consequently, optimization techniques are employed to identify the best possible solution among a set of feasible alternatives while satisfying the constraints imposed by the problem. [23.24]

In general, an optimization problem can be written as

optimize $f_1(x),\dots,f_i(x),\dots,f_N(x)$, $x=(x_1,\dots,x_d)$

subject to,

$$h_j(x)=0\ ,\ (j=1,2,\dots,J)$$

$$g_k(x)<=0\ ,\ ((k=1,\dots,K)$$

where f_1, ..., f_N are the objectives, while h_j and g_k are the equality and inequality constraints, respectively. In the case when N=1, it is called single-objective optimization. When N≥2, it becomes a multi-objective optimization problem whose solution strategy is different from those for a single objective. This article mainly concerns single-objective optimization problems.

III.2.3 Different types of optimization algorithms

III.2.3.1 Deterministic optimization algorithm

Deterministic approaches take advantage of the analytical properties of the problem to generate a sequence of points that converge to a globally optimal solution. These approaches can provide general tools for solving optimization problems to obtain a global or approximately global optimum.

Examples: linear programming, nonlinear programming, and mixed-integer nonlinear programming, etc.

III.2.3.2 Heuristics and metaheuristics

A metaheuristic is a high-level optimization strategy designed to guide and improve the search process for obtaining near-optimal solutions to complex optimization problems. Rather than solving a problem directly, it provides a framework for developing or selecting heuristics capable of efficiently exploring the search space. Metaheuristic methods are particularly useful when exact solutions are difficult to obtain due to the complexity of the problem, incomplete or uncertain information, or limited computational resources.[23]

Meta heuristics make relatively few assumptions about the optimization problem being solved and so may be usable for a variety of problems.

Examples:

- ✓ Particle Swarm Optimization (PSO),
- ✓ Ant Colony Optimization (ACO),
- ✓ Genetic Algorithms (GA),
- ✓ Cuckoo search algorithm,
- ✓ Grey wolf optimization (GWO)

This article aims to introduce the basics of a novel metaheuristic called Grey wolf optimization (GWO)

III.3 Grey wolf optimization (GWO) algorithm

III.3.1 Identification of GWO

The Grey Wolf Optimizer (GWO) is a population-based metaheuristic algorithm inspired by the social hierarchy and hunting behavior of grey wolves in nature. It was introduced [24,25]. The algorithm models the leadership structure and cooperative hunting strategy of grey wolf packs to effectively explore and exploit the search space.

Grey wolves are considered apex predators that occupy the highest level of the food chain. They typically live and hunt in organized social groups known as packs, which generally consist of 5 to 12 individuals. Within each pack, a strict social hierarchy is maintained, where members are classified according to their dominance and responsibilities during hunting and decision-making processes, as illustrated in the accompanying figure.

All the individuals in the group have a very strict social dominance hierarchy as demonstrated in the accompanying figure.

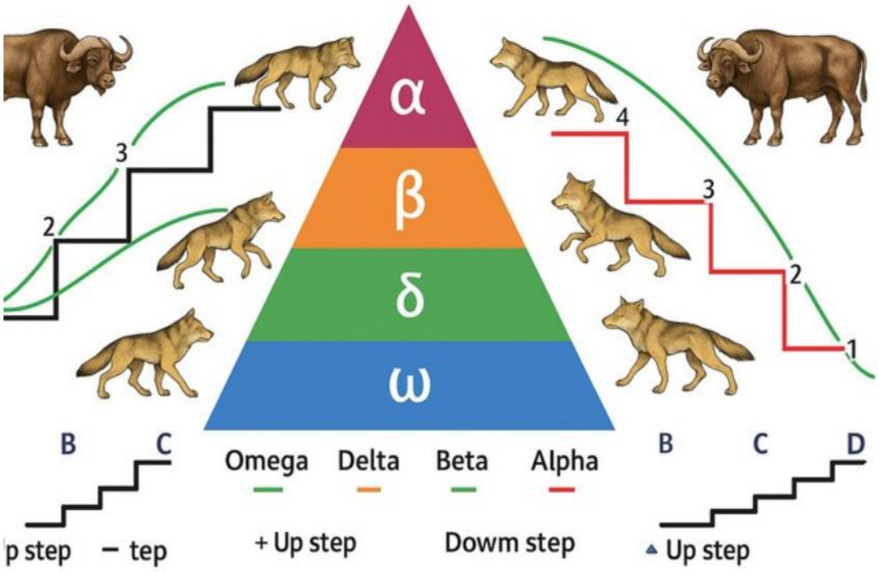

Figure III.5. GWO hierarchical categories.

In the Grey Wolf Optimizer (GWO), the social hierarchy of grey wolves is mathematically modeled through four main categories. The alpha (α) wolves represent the dominant individuals in the pack, whose decisions and guidance are followed by all other members. The beta (β) wolves act as subordinates to the alpha and assist in decision-making while also representing the most likely candidates to replace the alpha if necessary.

The delta (δ) wolves are subordinate to both alpha and beta wolves but dominate the omega group. They include various specialized roles such as scouts, sentinels, elders, hunters, and caretakers, each contributing to the overall functioning of the pack. Finally, the omega (ω) wolves are the lowest-ranking members of the hierarchy, often considered as scapegoats. They are the least dominant individuals in the group and typically feed last.

III.3.2 Main phases of grey wolf hunting

The hunting behavior of grey wolves is typically divided into three main stages: tracking and approaching the prey, pursuing and encircling it until it becomes immobilized, and finally executing the attack. These cooperative strategies, along with the social hierarchy of the pack, are mathematically modeled in the Grey Wolf Optimizer (GWO) to guide the search process toward optimal solutions.

III.3.3 Mathematical model and algorithm

III.3.3.1 Social hierarchy

- The Fittest solution as an Alpha wolf *(α)*
- Second best solution as a Beta wolf *(β)*
- Third best solution as a Delta wolf *(δ)*
- Rest of the candidate solutions as Omega wolves (ω)

III.3.3.2 Encircling the Prey

$$\vec{D} = | \vec{C}.\overrightarrow{X_p}(t) - \overrightarrow{X_p}(t) | \tag{III.29}$$

$$\vec{X}(t+1) = \overrightarrow{X_p}(t) - \vec{A}.\vec{D} \tag{III.30}$$

Where t indicates the current iteration, $\vec{A}$ and $\vec{C}$ are coefficient vectors, $\overrightarrow{X_p}$ is the position vector of the prey, and $\vec{X}$ indicates the position vector of a grey wolf.$\overrightarrow{X_1}(t+1) = \overrightarrow{X_\alpha}(t) - \overrightarrow{A_1}.\overrightarrow{D_\alpha}$

$$\vec{A} = 2\vec{a}\overrightarrow{r_1} - \vec{a} \quad \text{and} \quad \vec{C} = 2\overrightarrow{r_2} \tag{III.31}$$

components of $\vec{a}$ are linearly decreased from 2 to 0 over the course of iterations and $\overrightarrow{r_1}$, $\overrightarrow{r_2}$ are random vectors in [0, 1].

III.3.3.3 Hunting

In each iteration, omega wolves update their positions in accordance with the positions α, β, and δ alpha, beta, and delta because α, β, and δ have better knowledge about the potential location of prey.

$$\begin{cases} \overrightarrow{D_\alpha} = | \overrightarrow{C_1}.\overrightarrow{X_\alpha}(t) - \vec{X}(t) | \\ \overrightarrow{D_\beta} = | \overrightarrow{C_2}.\overrightarrow{X_\beta}(t) - \vec{X}(t) | \\ \overrightarrow{D_\delta} = | \overrightarrow{C_3}.\overrightarrow{X_\delta}(t) - \vec{X}(t) | \end{cases} \quad \text{(III.32)}$$

$$\begin{cases} \overrightarrow{X_1}(t+1) = \overrightarrow{X_\alpha}(t) - \overrightarrow{A_1}.\overrightarrow{D_\alpha} \\ \overrightarrow{X_2}(t+1) = \overrightarrow{X_\beta}(t) - \overrightarrow{A_2}.\overrightarrow{D_\beta} \\ \overrightarrow{X_3}(t+1) = \overrightarrow{X_\delta}(t) - \overrightarrow{A_3}.\overrightarrow{D_\delta} \end{cases} \quad \text{(III.33)}$$

$$\vec{X}(t+1) = (\overrightarrow{X_1} + \overrightarrow{X_2} + \overrightarrow{X_3})/3 \quad \text{(III.34)}$$

III.3.3.4 Attacking prey (exploitation)

When prey stops moving then grey wolf finish the hunting by attacking the prey and to mathematically model that we decrease the value of $\vec{a}$. $\vec{A}$ is a random value in the interval [-2a, 2a], where a is decreased from 2 to 0 over course of iterations.

|A|<1 force the wolves to attack the prey (exploitation)

III.3.3.5 Searching for prey (exploration)

|A|>1 forces the grey wolves to diverge from the prey to hopefully find a fitter prey (exploitation)

Another component of GWO that favours exploration is $\vec{C}$. It contains random value between [0, 2]. C>1 emphasize the attack while C<1 deemphasize the attack.

III.4 Pseudocode of the GWO algorithm

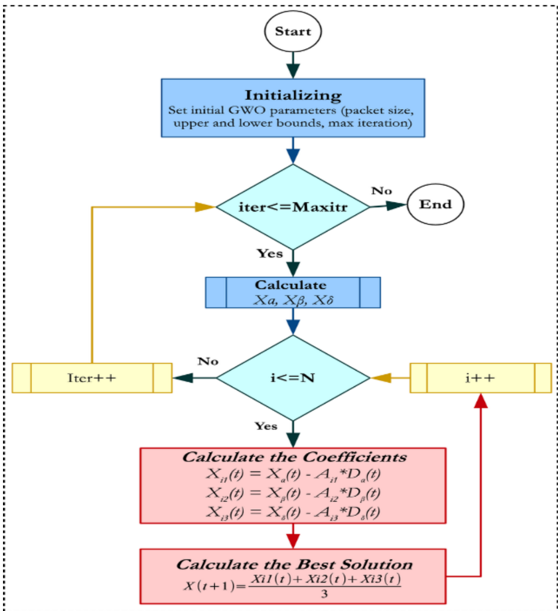

Figure III.6. The flowchart of the GWO algorithm.

III.7 Simulation Results

The modeling and simulation of the PMSM drive system, as well as the proposed control schemes, were carried out in the MATLAB/Simulink environment. Table A.1 presents the parameters of the PMSM.

III.7.2 Simulation Results for 600 rpm and Load Torque Variation

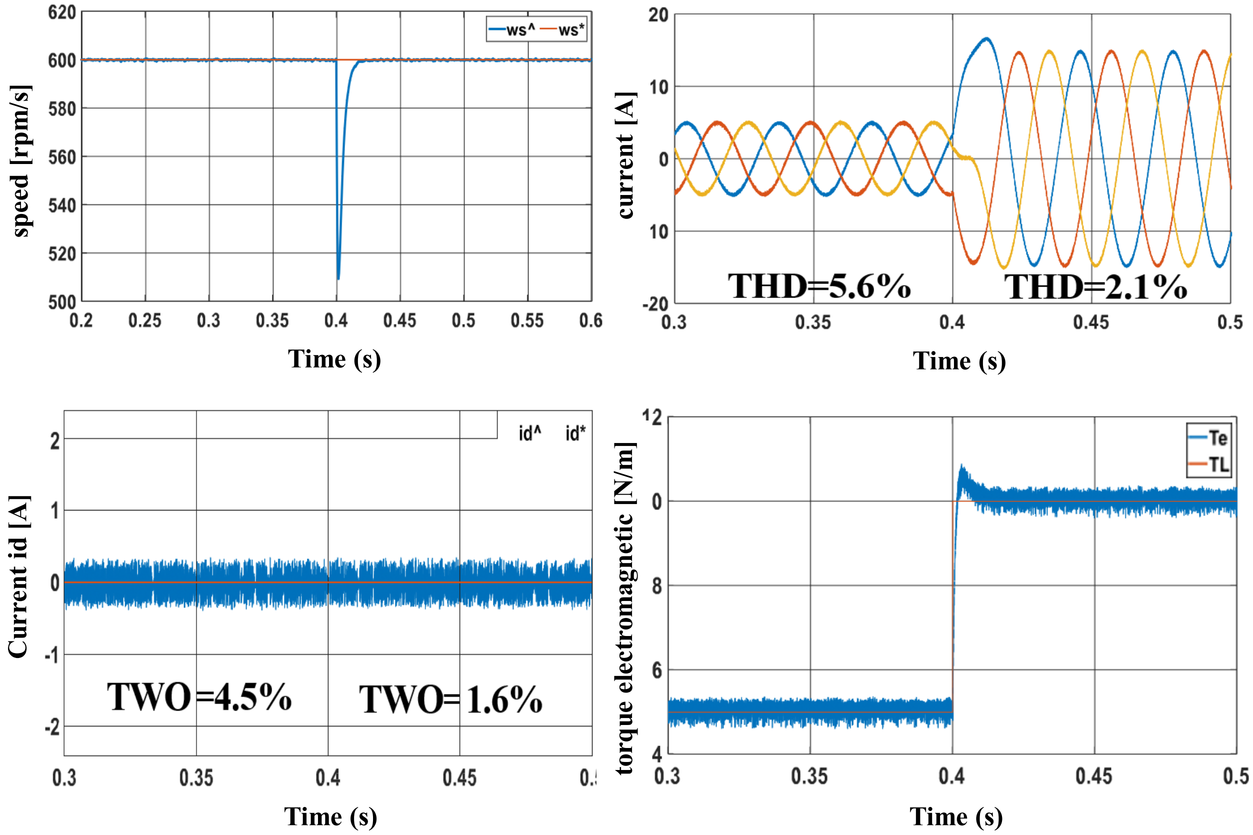

Figure III.7. Classical predictive current control with nominal parameters.

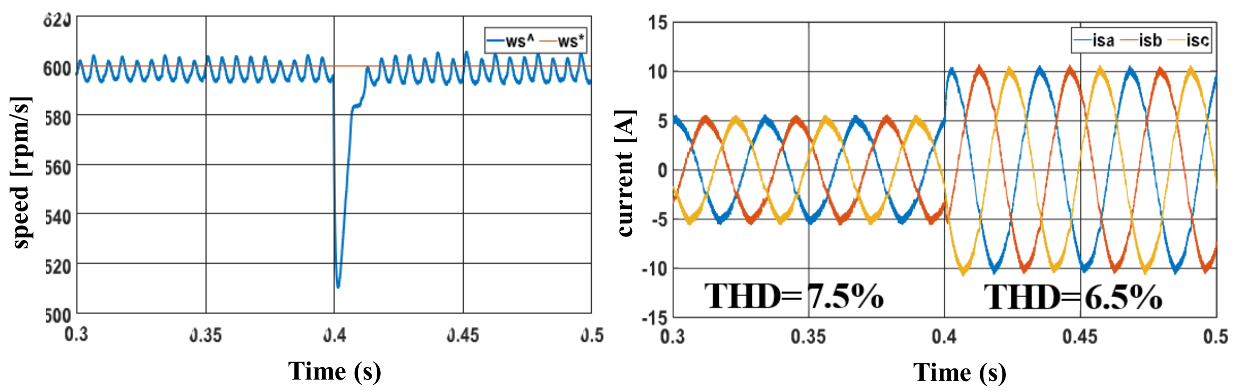

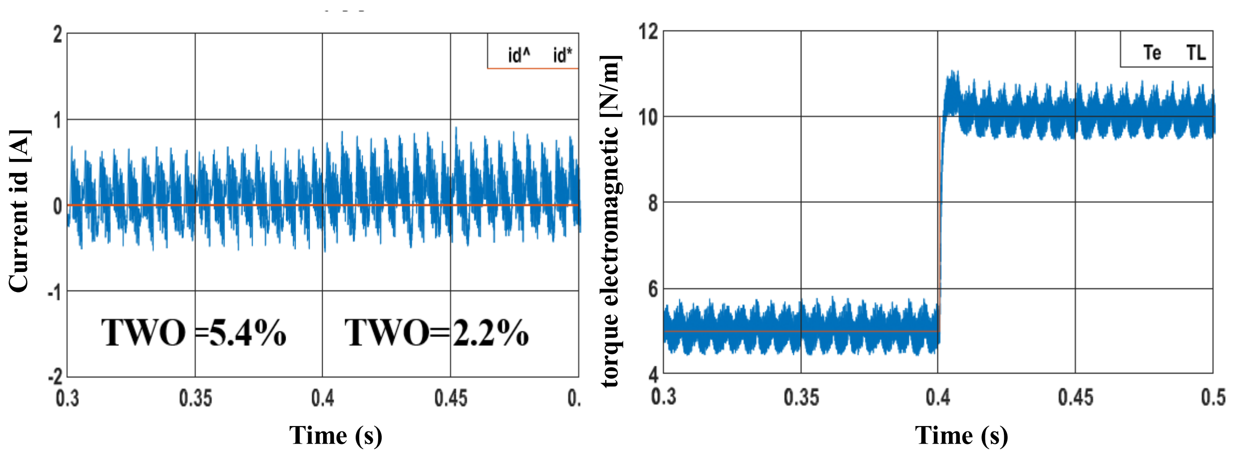

Figure III.8. Classical predictive current control under the influence of parameter variations

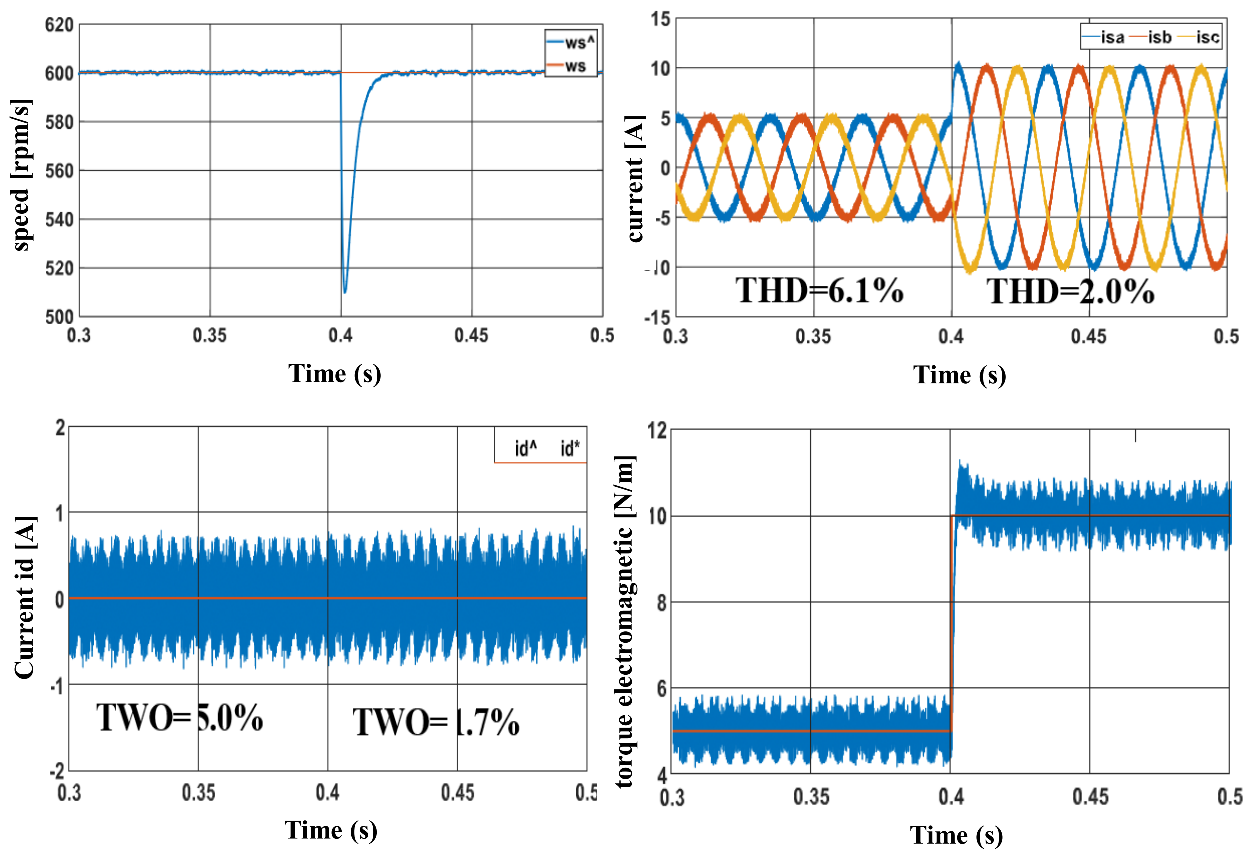

Figure III.9. Advanced predictive current control.

To better evaluate the dynamic performance of the studied control strategies, comparative tests were carried out and are presented in Figure 3.7, where a load torque is applied instantaneously at time t=0.4 s, increasing from 5 Nm to 10 Nm, with a constant speed reference of 600 rpm. It is observed that all control strategies achieve a fast dynamic response, and the rotor speed follows its reference with good stability and accuracy after a slight drop due to the load step.

Regarding current performance, the enlarged steady-state waveforms show that the advanced predictive current control presents sinusoidal current waveforms, similar to those of classical predictive current control with nominal parameters, with a slight difference in THD values (see Figure 3.7, Figure 3.9). It is evident that the advanced predictive current control offers better performance than the classical predictive current control in terms of d-axis current in steady state, ensuring smooth and accurate reference tracking.

In contrast, the advanced predictive current control shows slightly inferior performance on the q-axis compared to classical predictive current control, with a minimal difference in THD, but it still provides perfect reference tracking capability. On the other hand, since classical predictive current control strongly depends on parameter accuracy, it is impossible to obtain sinusoidal current waveforms when mismatched inductances are assumed, as shown in Figure 3.8, resulting in poor THD performance.

The dq-axis currents exhibit the worst ripples in steady state, leading to high THD values, and a significant deviation in the q-axis current is observed, which increases as the load torque increases. From the considered control strategies, it can be concluded that the performance of classical predictive current control with incorrect parameters degrades increasingly as the load torque increases. In contrast, the proposed advanced predictive current control demonstrates high immunity to PMSM parameter variations and strong robustness against sudden and large load torque variations.

III.7.3 Simulation Results for 1500 rpm with Speed and Load Torque Variations

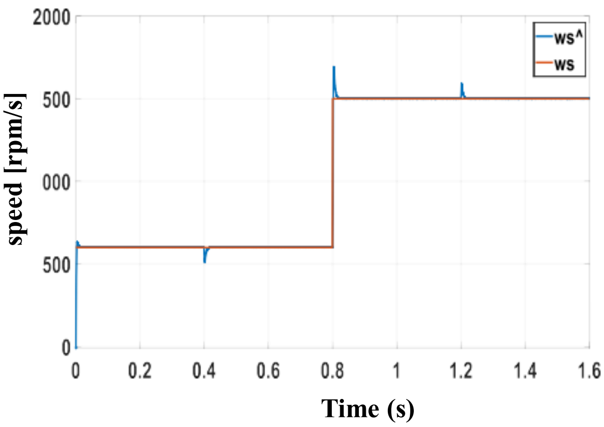

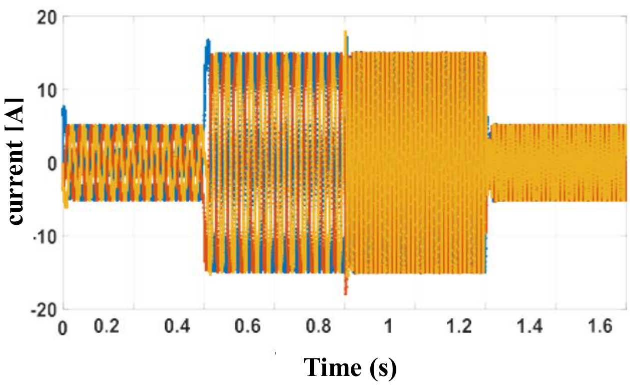

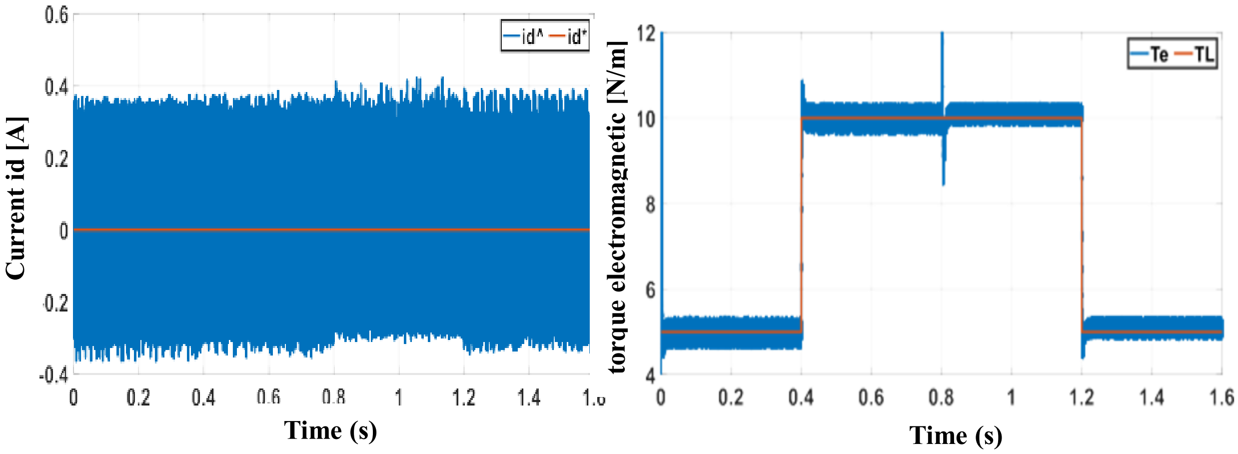

Figure III.10. Classical Predictive Current Control with Nominal Parameters.

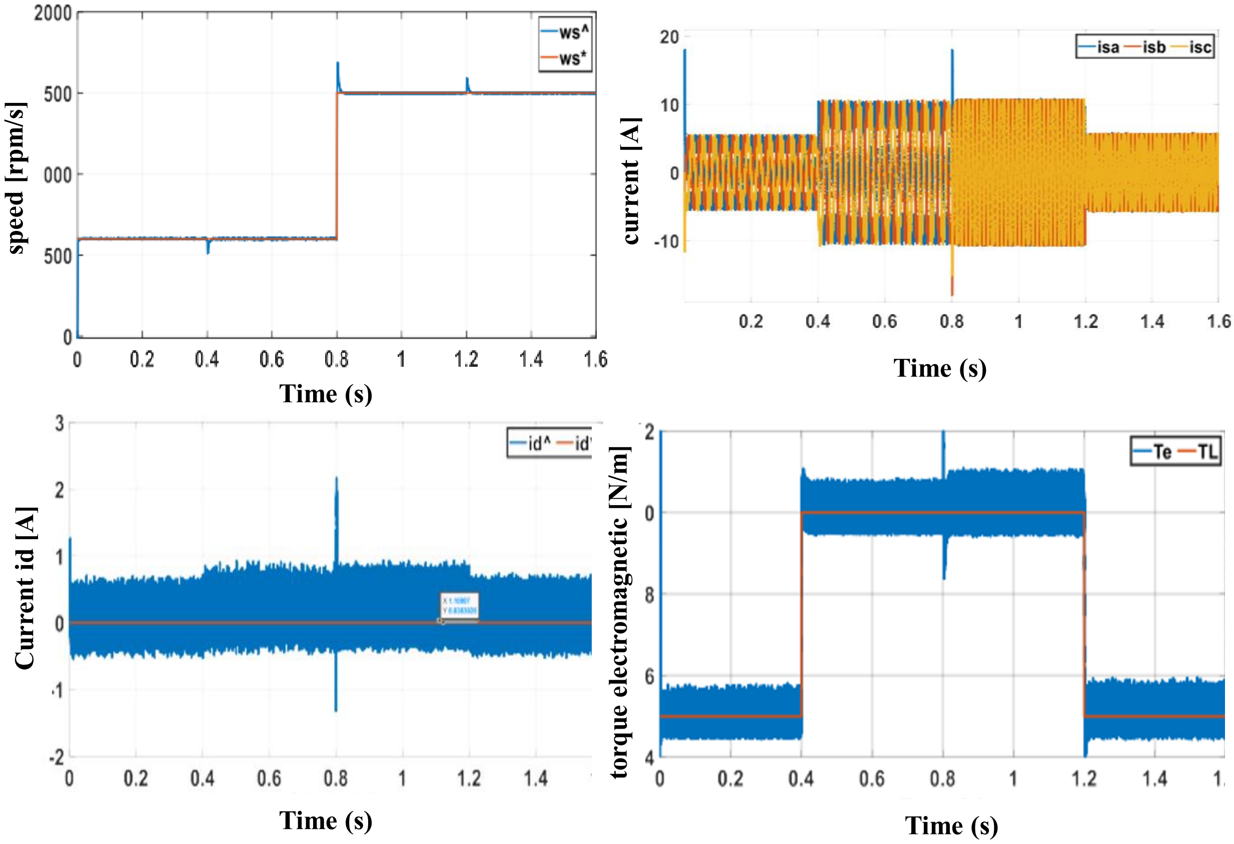

Figure III.11. Classical predictive current control under the influence of parameter variations.

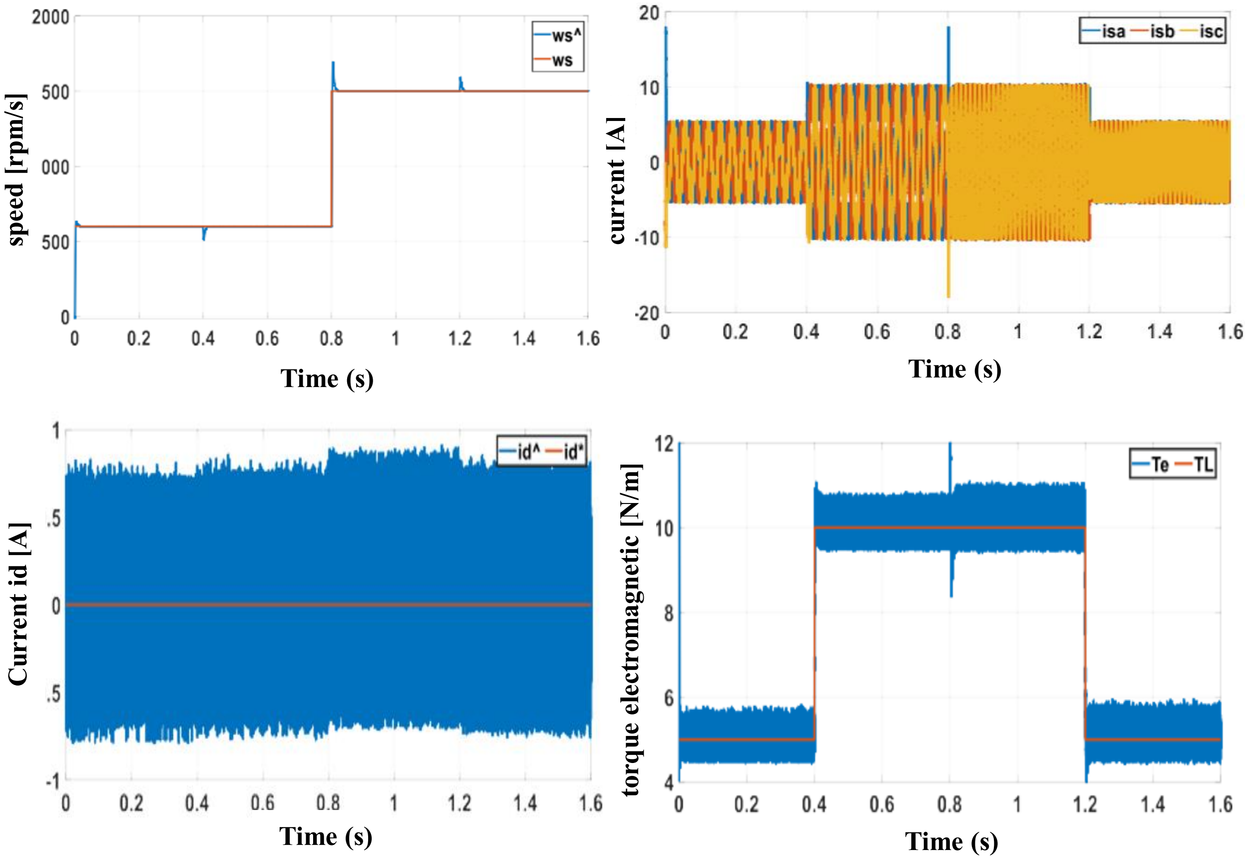

Figure III.12. Advanced predictive current control.

Figure 3.10 presents the simulation results of classical predictive current control and advanced predictive current control under the same operating conditions. Initially, the reference speed is set to 600 rpm with a load torque of 5 N·m. Then, at t = 0.8 s, the reference speed is increased to 1500 rpm, while at t = 0.4 s, the load torque is increased to 10 N·m.

The performance of classical predictive current control with nominal parameters is illustrated in Figure 3.10. The first and second plots show the actual PMSM currents, the third plot presents the d-axis and q-axis currents together with their references, and the last plot shows the rotor speed and its reference value.

From the results, it can be clearly observed that even when nominal parameters are used, a noticeable deviation appears in the q-axis current with respect to its reference, and this deviation increases as both the speed and the load torque increase. Classical predictive current control is sensitive to parameter variations; therefore, the q-axis current tracking error becomes even larger when inductance variations are introduced by setting the d-axis and q-axis inductances below their nominal values, as shown in Figure 3.11.

As a result, significant current ripples and harmonic distortions are observed, particularly under inductance variations. It should be emphasized that the inductance variation is introduced by modifying the inductance values within the classical predictive current control algorithm.

In contrast, since the advanced predictive current control does not require knowledge of the motor parameters, the q-axis current tracking error is eliminated, demonstrating an inherent immunity to PMSM parameter variations. Consequently, although both control schemes achieve a fast dynamic response and provide similar rotor-speed performance, the investigated advanced predictive current control exhibits superior harmonic distortion performance.

III.8 Conclusion

This chapter presents an advanced predictive current control strategy based on real-time current measurements and employing the Grey Wolf Optimizer (GWO) algorithm. The proposed control scheme consists of two main processes:

1. The proposed discrete model does not rely on any machine parameters and does not require knowledge of the motor parameters. It only requires the optimal factor to generate the predictions of the d-axis and q-axis currents, thereby avoiding the influence of parameter variations.

2. The cost function evaluates the error between the reference currents and the predicted currents. The GWO algorithm then searches for the minimum value of the cost function to determine the optimal factor to be applied at the next sampling instant.

The proposed advanced predictive current control is compared with classical predictive current control. The simulation results show that both control schemes provide excellent dynamic performance. However, unlike classical predictive current control, which is susceptible to parameter variations, the advanced predictive current control is unaffected by motor parameter uncertainties and is capable of achieving better steady-state performance.

Furthermore, the tracking capability of the proposed method confirms its robustness, while the small difference in execution time between the advanced predictive control method and the classical predictive control method (25.5 µs for the classical predictive current control and 28.5 µs for the advanced predictive current control) demonstrates the efficiency of the proposed approach compared with other advanced predictive control techniques.

The results confirm the effectiveness of the proposed method by exhibiting superior overall performance in terms of current ripple reduction and tracking-error minimization under various operating conditions. Based on the presented results, it can be concluded that the proposed technique represents a promising alternative to model-based predictive control schemes, particularly when insufficient motor data are provided by the manufacturer and when self-commissioning procedures are difficult to implement.

.

General Conclusion

General Conclusion

In conclusion, this thesis has presented a comprehensive investigation into the modeling and predictive current control of a Permanent Magnet Synchronous Motor (PMSM) supplied by a two-level three-phase voltage source inverter for electric traction applications. Owing to their high efficiency, high power density, excellent torque characteristics, and reduced maintenance requirements, PMSMs have become one of the most attractive solutions for modern electric vehicle propulsion systems. Consequently, the development of advanced control strategies capable of maximizing their performance and robustness remains a significant research challenge.

A detailed mathematical model of the PMSM was established using the abc, αβ, and dq reference-frame transformations, providing an effective framework for analyzing the machine dynamics and designing advanced control algorithms. The complete drive system, including the power converter and the PMSM, was modeled in the MATLAB/Simulink environment to evaluate the performance of different predictive current control strategies under realistic operating conditions.

Particular emphasis was placed on the study of Model Predictive Current Control (MPCC) and its limitations regarding parameter sensitivity. While conventional predictive current control offers excellent dynamic performance and fast current regulation, its effectiveness strongly depends on the accuracy of the machine parameters used in the prediction model. Variations in stator resistance and inductances may significantly degrade current-tracking performance, increase harmonic distortion, and reduce overall control quality.

To overcome these limitations, an advanced predictive current control strategy based on real-time current measurements and the Grey Wolf Optimizer (GWO) algorithm was proposed and investigated. Unlike conventional model-based predictive approaches, the proposed method does not require precise knowledge of the PMSM parameters, thereby eliminating the adverse effects of parameter mismatches and uncertainties. The optimization process continuously determines the optimal control factor by minimizing a cost function based on current-tracking errors, resulting in improved robustness and steady-state performance.

Extensive simulation studies were carried out under various operating conditions, including speed variations, load torque disturbances, and parameter uncertainties. The obtained results demonstrated that both conventional and advanced predictive control strategies achieve rapid dynamic responses and satisfactory speed-tracking performance. However, the proposed advanced predictive current control exhibited superior robustness against parameter variations, reduced current ripples, lower harmonic distortion, and improved current-tracking accuracy. Furthermore, despite the integration of the GWO optimization algorithm, the increase in computational burden remained relatively small, confirming the practical feasibility of the proposed approach for real-time applications.

Overall, the results validate the effectiveness of the proposed advanced predictive current control scheme as a promising alternative to conventional model-based predictive controllers, particularly in applications where motor parameters are uncertain, unavailable, or subject to significant variations during operation.

As future work, several research directions can be considered, including the implementation of the proposed controller on real-time hardware platforms such as DSPs, FPGAs, or embedded controllers, the investigation of multi-objective cost functions for simultaneous optimization of current quality and switching losses, the extension of the approach to multilevel inverter topologies, and the integration of artificial intelligence techniques to further enhance the adaptability, robustness, and efficiency of PMSM drive systems for next-generation electric vehicle applications.

.

Appendix A

Symbols	Description	Values	Units
(R_s)	Stator resistance	0.7	(Ω)
(L_{sd})	Direct-axis inductance	0.007	H
(L_{sq})	Quadrature-axis inductance	0.007	H
(J)	Motor inertia	0.0700	kg·m²
(B_M)	Friction coefficient	0.000629	N·m/rad/s
(p)	Number of pole pairs	3	—
(P_N)	Rated power	7.4	kW
(N_n)	Rated speed	3000	tr/min
(T_n)	Rated load torque	23.4	N·m
(I_n)	Rated current	14.7	A
(V)	Voltage	220/380	V
(ψ_n)	Rotor flux	0.225	Wb

Bibliography

References

[1] S. E. Labiod, "Study of a wind energy system based on a permanent magnet synchronous machine," Master's thesis, 2022–2023.

[2] M. B. Medjed Eddine and M. B. Imad Eddine, "Study and implementation of a wind energy system based on a permanent magnet synchronous machine," Master's thesis, 2024.

[3] H. Mensous and S. Sallaye, "Modeling and simulation of a wind turbine based on a doubly fed induction machine," Master's thesis, 2020–2021.

[4] A. Tobías-González, R. Peña-Gallardo, J. Morales-Saldaña, and G. Gutiérrez-Urueta, "Modeling of a wind turbine with a permanent magnet synchronous generator for real-time simulations," Facultad de Ingeniería, Universidad Autónoma de San Luis Potosí, San Luis Potosí, Mexico.

[5] D. Ssemanda, "Vector control of the permanent magnet synchronous machine," Master's thesis, Université Saad Dahlab de Blida, 99 pp., 2015–2016.

[6] A. de Almeida and S. Greenberg, "Electric motors," in *Encyclopedia of Energy*, 2004, pp. 191–201.

[7] ParkingPreheater, "Introduction to permanent magnet synchronous motors." Online article.

[8] S. Arif and A. Bouchaala, "Control of the permanent magnet synchronous machine using artificial neural networks," Master's thesis, Université Kasdi Merbah Ouargla, 106 pp., 2018–2019.

[9] Wevolver, "Understanding process control: An important technique for industrial processes." Online article.

[10] MATLAB, "Understanding field-oriented control | Motor control, Part 4," YouTube video.

[11] R. M. Murray, *Control and Dynamical Systems*, California Institute of Technology.

[12] F. Z. Hanbli and N. Laidouni, "Robust control of a permanent magnet synchronous generator used in a wind energy conversion chain," Master's thesis, 2024–2025.

[13] T. Merzougui and K. Abdelkebir, "Control of a permanent magnet synchronous generator," Master's thesis, 2018–2019.

[14] "Design of a permanent magnet synchronous generator for a vertical axis wind turbine," Master of Science thesis in Electrical Machines and Power Electronics, School of Electrical Engineering, Royal Institute of Technology, Stockholm, Sweden, Jun. 2011.

[15] A. Laidani and O. A. Litim, "Advanced control of a permanent magnet synchronous generator integrated into a wind energy system," Master's thesis, 2023.

[16] N. E. I. Cheni, M. Baouia, and A. Atoussi, "Vector control of an autonomous permanent magnet synchronous generator connected to DC microgrids without a storage system," Master's thesis, 2024–2025.

[17] M. Mayouf, "Comparative study of architectures and control strategies for a permanent magnet synchronous wind generator," Université El Hadj Lakhdar, Batna, 2014.

[18] I. Meghlaoui, "Modeling and simulation of a low-power horizontal-axis wind energy conversion chain," Magister thesis, Université Badji Mokhtar, Annaba, 2009.

[19] S. E. Ziraoui, "Modeling and study of a grid-connected wind energy system," Master's thesis, Université Badji Mokhtar, Annaba, 2017.

[20] STMicroelectronics, "Sensorless field-oriented control for a permanent magnet synchronous motor using a sliding mode observer," Application Note AN4398.

[21] Scribd, "Sensorless FOC: Techniques and challenges." Online document.

[22] "An improved grey wolf optimization algorithm with variable weights," *Computational Intelligence and Neuroscience*, vol. 2019, Art. ID 2981282, 13 pp., 2019.

[23] S. Mirjalili, S. M. Mirjalili, and A. Lewis, "Grey wolf optimizer," *Advances in Engineering Software*, vol. 69, pp. 46–61, 2014.

[24] Y. Li, M. Han, and Q. Guo, "An improved grey wolf optimization algorithm to solve engineering optimization problems," *Sustainability*, vol. 13, no. 6, Art. no. 3208, 2021.

[25] K. Benamara *et al.*, "Grey wolf optimization for enhanced performance in wind power systems," *Frontiers in Energy Research*, vol. 12, 2024.

[26] A. G. Abo-Khalil, A. S. Alghamdi, and I. Tlili, "Fuzzy logic control of wind energy conversion system," *Journal of Renewable and Sustainable Energy*, vol. 5, no. 2, 2013.

[27] P. J. Costa, "Fuzzy logic as a method to optimize wind systems," in *Wind Power Systems*, Springer, 2010.

[28] A. Maafa *et al.*, "Fuzzy logic-based smart control of wind energy conversion systems," *Sustainability*, vol. 16, no. 21, 2024.

[29] N. Huang, "Simulation of power control of a wind turbine permanent magnet synchronous generator system," Master of Science thesis, Department of Electrical and Computer Engineering, Marquette University, USA, 2013.

[30] A. Li, "Engineering aerodynamic models for horizontal-axis wind turbines," Master's thesis, Technical University of Denmark, Denmark, 2021.

[31] V. Mendoza, "Aerodynamic studies of vertical axis wind turbines using the actuator line model," Ph.D. dissertation, Uppsala University, Sweden, 2018.

[32] S. M. Barakati, "Modeling and controller design of a wind energy conversion system including a matrix converter," Ph.D. dissertation, University of Waterloo, Canada, 2008.